Journal of Medicinal Chemistry

pubs.acs.org/jmc

Article

Identifying Structural Factors Governing the Photodynamic Activity of Phthalocyanines

Magdalena Kozlikova,[‡] Mary Angelia Alfred,[‡] Miloslav Machacek,*[,‡] Fabienne Dumoulin, Andrés de la Escosura, Tomasz Goslinski, Marie Halaskova, Jian-Dong Huang, Mei-Rong Ke, Saad Makhseed, Dariusz T. Mlynarczyk, Dennis K. P. Ng, Tomás Torres, Roy C. H. Wong, Petr Zimcik,* and Veronika Novakova*

Cite This: *J. Med. Chem.* 2026, 69, 4391−4407

Read Online

ACCESS | Metrics & More | Article Recommendations | Supporting Information

ABSTRACT: Phthalocyanines (Pcs) are promising photosensitizers (PSs) for photodynamic therapy (PDT). However, the variability in experimental conditions in *in vitro* experiments among reported derivatives complicates clear comparisons. In this study, we systematically evaluated a diverse set of more than 40 cationic, anionic, nonionic Zn, Mg, or metal-free or axially substituted silicon Pcs and compared them under standardized conditions. Their spectral and photophysical properties, interactions with bovine serum albumin, subcellular localization, and *in vitro* PDT efficacy in three human cancer cell lines were assessed. Structural features influencing PDT efficacy include their presence in the monomeric state through axial substitution (in silicon Pcs) or rigid bulky peripheral groups with the latter enhancing activity in cationic derivatives while reducing it in nonionic derivatives. Amphiphilic structures significantly improved the PDT efficacy, especially for nonionic and anionic Pcs. The results of this study provide clear design principles for the future development of highly efficient PSs for PDT.

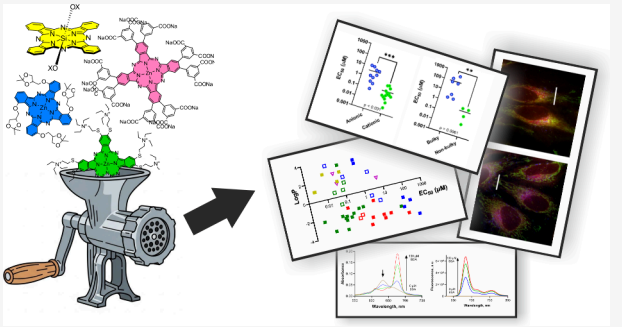

INTRODUCTION

Photodynamic therapy (PDT) has emerged as a promising minimally invasive treatment modality for cancer. Its principle is based on the accumulation of a photosensitizer (PS) in cancerous tissues, followed by its activation with light of a specific wavelength. This activation leads to the generation of reactive oxygen species, primarily singlet oxygen ($^1O_2$), which induce cytotoxic effects and ultimately lead to cancer cell death. Many structural types of PSs have been shown to have photodynamic properties, and mainly the representatives of porphyrins and phthalocyanines (Pcs) have been used in clinical cancer treatment.[1] This is probably due to their unique spectral and photophysical properties (i.e., high singlet oxygen production), good photostability, and the possibility of fine-tuning their properties (e.g., water solubility, aggregation suppression, and position of absorption maxima). Compared with porphyrins, Pcs have the advantage of strong absorption in the far-red and near-infrared regions of the visible spectrum, enabling deeper penetration of activating light through the tissues. This is why interest in these macrocycles is growing exponentially.[2,3]

As of June 2025, more than 5,300 publications related to the use of Pcs in PDT have been indexed in the Web of Science (search terms: *phthalocyanine*, *photodynamic*). Of these, approximately 1,500 reports include *in vitro* investigations (additional search term: *in vitro*). Collectively, this body of literature constitutes a substantial resource that, in principle, could enable the identification of key structural determinants and the rational design of optimized therapeutic candidates. However, deriving such conclusions remains challenging because of the considerable heterogeneity in the experimental conditions used across *in vitro* studies, including the type of light source (LEDs, lasers, or broad-spectrum lamps), irradiation intensity, incubation time of Pcs with cells, drug-to-light interval, irradiation duration, and choice of cell lines. Consequently, reported values of the half-maximum effective concentration (EC_{50}) are often not directly comparable across studies.

To address the limitations associated with cross-study comparisons, more than 40 representative Pcs with a variety of substitutions (Figure 1), which have already been reported to show favorable photodynamic properties, were analyzed.

Received: October 23, 2025
Revised: January 2, 2026
Accepted: January 23, 2026
Published: February 6, 2026

https://doi.org/10.1021/acs.jmedchem.5c03090
J. Med. Chem. 2026, 69, 4391−4407

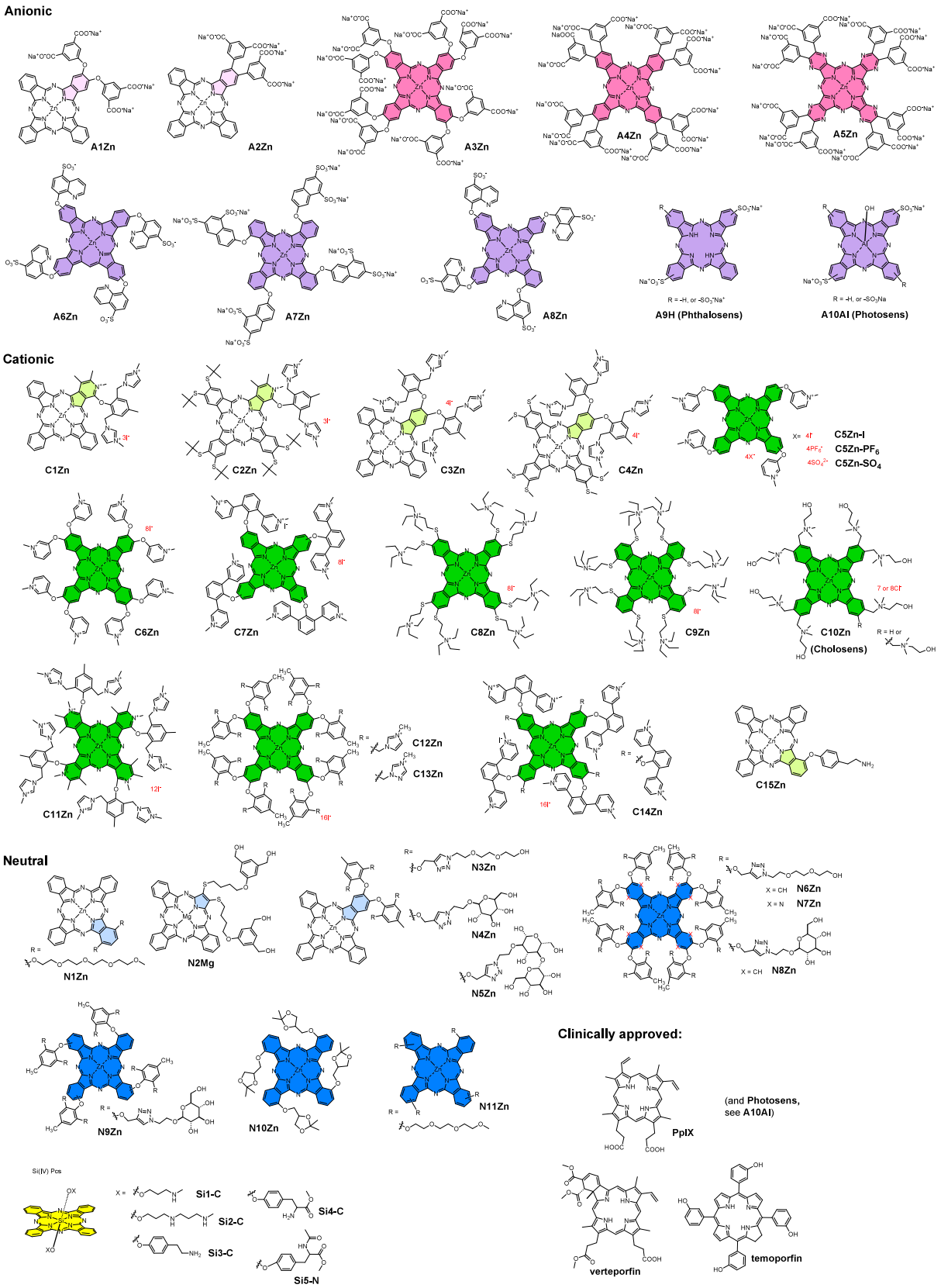

Figure 1. Structures of the compounds involved in the study. Color code always indicates the isoindole unit that is modified with the hydrophilic substituent. Light version of the color stresses the unsymmetrical composition of the substitution. Pink – anionic Pcs with carboxylic function, magenta – anionic Pcs with sulfonate functions, green – cationic Pcs, blue – nonionic Pcs, yellow – silicon Pcs, irrespective of the axial substitution. Note: **C10Zn** (known as Cholosens) is a mixture of Zn(II)Pcs having either seven or eight *N*-(2-hydroxyethyl)-*N*,*N*-dimethylammoniomethyl groups with an average substitution degree of 7.5.

https://doi.org/10.1021/acs.jmedchem.5c03090
J. Med. Chem. 2026, 69, 4391−4407

Table 1. Photophysical Data of Investigated Derivatives in DMF[a]

Cpd.	λ_A/nm	ε/M^{-1}cm^{-1}	λ_F/nm	Φ_F	τ_{F1}/ns	τ_{F2}/ns	Φ_Δ	Log P	Synthesis in ref
A1Zn	673	165 600	682	0.035	0.44 (15%)	2.51 (85%)	0.26	−2.70	17
	681	164 000							
A2Zn	677	152 090	688	0.02	0.23 (16%)	2.66 (84%)	0.22	−2.42	17
A3Zn	677	172 640	688	0.03 (0.19)[b]	0.82 (18%)	2.57 (82%)	0.24 (0.42)[b]	−2.88	17
A4Zn	694	168 630	708	0.01 (0.12)[b]	0.36 (4%)	2.78 (96%)	0.45 (0.45)[b]	−3.32	17
A5Zn	659	138 740	675	0.03	0.20 (56%)	1.11 (44%)	0.21	−3.27	17
A6Zn	681	122 420	692	0.28	3.14		0.58	−2.89	18
A7Zn	696	109 950	707	0.23	2.57		0.55	−2.92	19
A8Zn	696	197 610	708	0.26	2.83		0.69	−3.64	18
A9H[c]	694, 662	104 650	703	0.22	1.97 (18%)	3.87 (82%)	0.19	−1.35	20
A10Al[d]	711, 688	105 250	717	0.62	4.14 (3%)	5.60 (97%)	0.25	−1.20	20
C1Zn	689	100 240	696	0.15	1.88		0.66	0.53	17
C2Zn	708	177 880	718	0.30	1.67		0.70	1.38	10
C3Zn	673	177 190	682	0.19	2.47		0.53	−0.84	17
C4Zn	697	106 360	709	0.21	1.64		0.44	0.62	10
C5Zn-I	674	130 860	682	0.25	2.38 (97%)	6.53 (3%)	0.49	−2.19	21
C5Zn-PF$_6$	674	86 800	682	0.28	2.32 (97%)	6.31 (3%)	0.45	−2.37	22
C5Zn-SO$_4$	674	82 140	682	0.08	2.47 (94%)	4.93 (6%)	0.28	−3.57	21
C6Zn	681	41 730	683	0.001	0.07 (3%)	2.84 (97%)	0.02	−2.59	23
C7Zn	684	121 730	693	0.23	2.07 (95%)	4.86 (5%)	0.37	−2.47	24
C8Zn	704	281 600	714	0.29	1.52 (14%)	2.41 (86%)	0.63	−1.59	25
C9Zn	757	134 170	783	0.06	0.62 (8%)	1.14 (92%)	0.64	−1.65	25
C10Zn	686	40 580	695	0.12	1.56 (25%)	2.37 (75%)	0.41	−2.03	20
C11Zn	716	160 750	726	0.21	1.41		0.53	−2.25	17
C12Zn	679	244 030	687	0.20	0.62 (7%)	2.23 (93%)	0.48	−2.08	26
C13Zn	679	236 490	687	0.20	0.60 (4%)	2.27 (96%)	0.37	−3.47	27
C14Zn	690	222 730	698	0.22	0.79 (34%)	2.04 (66%)	0.40	−2.38	24
C15Zn	675	136 590	684	0.20	1.23 (7%)	2.96 (93%)	0.53	3.32	8
N1Zn	689	82 550	702	0.24	2.41		0.67	3.52	28
N2Mg	684	15 950	687	0.16	1.29 (25%)	3.39 (75%)	0.17	1.97	29
N3Zn	672	280 340	681	0.28	3.43		0.48	1.90	30
N4Zn	672	293 750	681	0.29	3.52		0.59	−0.65	30
N5Zn	672	209 500	681	0.28	3.44		0.47	−1.33	30
N6Zn	681	237 520	690	0.26	1.04 (3%)	3.17 (97%)	0.46	−2.59	31
N7Zn	629	195 490	641	0.18	0.74 (5%)	2.45 (95%)	0.58	−1.60	31
N8Zn	680	275 660	689	0.25	3.30		0.45	−3.64	32
N9Zn	700	248 160	712	0.24	2.63		0.57	−2.02	32
N10Zn	697	147 000	708	0.23	2.34		0.68	3.48	33
N11Zn	699	146 930	710	0.21	2.43		0.53	3.10	34
Si1-C	676	214 560	683	0.15	1.00 (50%)	4.50 (50%)	0.20	2.44	35
Si2-C	671	229 280	679	0.25	1.00 (9%)	5.15 (91%)	0.23	1.64	35
Si3-C	680	204 080	687	0.06	0.55 (65%)	4.63 (35%)	0.05	2.57	8
Si4-C	680	236 170	689	0.07	0.96 (96%)	2.28 (4%)	0.06	2.69	36
Si5-N	680	132 950	689	0.10	1.23 (69%)	1.68 (31%)	0.085	1.05	36
PpIX	630		634	0.12	1.79 (20%)	13.8 (80%)	0.73[e]	1.06	commercial
verteporfin	690		696	0.18	6.05		0.75[e]	2.51	commercial
temoporfin	651		656	0.24	9.66		0.76[e]	1.40	commercial

[a]Absorption maximum in the Q-band (λ_A); extinction coefficient (ε); fluorescence emission maximum (λ_F); fluorescence quantum yield (Φ_F) determined by the comparative method using unsubstituted zinc phthalocyanine as reference (Φ_F(ZnPc) = 0.32 in THF); fluorescence lifetime (τ_F); quantum yield of singlet oxygen production (Φ_Δ) determined by the comparative method using unsubstituted zinc phthalocyanine (Φ_Δ(ZnPc) = 0.56 in DMF) for all studied Pcs or Rose Bengal (RB) (Φ_Δ(RB) = 0.47 in DMF for PpIX, verteporfin, and temoporfin) as reference and DPBF as a scavenger; experimentally determined partition coefficient between 1-octanol and PBS in logarithmic scale (log P). [b]Determined for their nonionized analogues containing free carboxylic acid; value taken from ref 17. [c]Phthalosense. [d]Photosens. [e]With RB as reference.

Their photophysical characteristics and photodynamic efficacy *in vitro* on three cell lines were systematically evaluated under standardized experimental conditions. Through this comprehensive comparative experimental study, we aimed to elucidate the basic structure−activity relationships underlying the efficacy of Pcs in PDT, ultimately leading to structural recommendations for the development of more effective PSs for cancer treatment.

https://doi.org/10.1021/acs.jmedchem.5c03090
J. Med. Chem. 2026, 69, 4391−4407

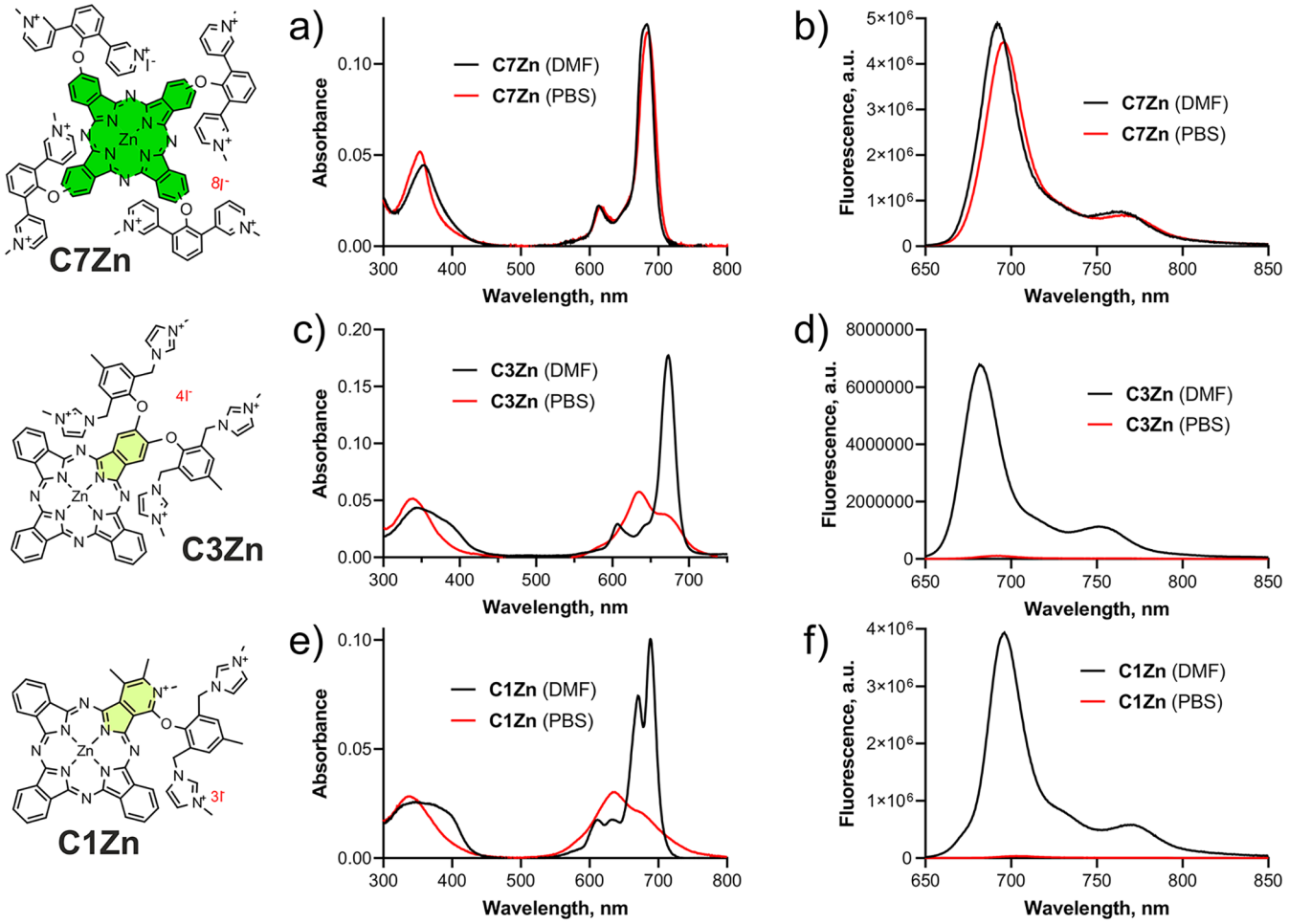

Figure 2. Representative examples (c = 1 μM) of absorption (a, c, e) and fluorescence emission spectra (b, d, f) of compound **C7Zn**, which is monomeric in both DMF and aqueous medium (e.g., PBS) (a, b); **C1Zn** and **C3Zn**, which are monomeric in DMF but are aggregated in PBS (c, d, e, f), and compound **C1Zn** having a split Q-band in monomeric form (e, black line). Spectra of all compounds of the series are shown in Supporting Information Figures S1−S43.

RESULTS AND DISCUSSION

Compounds Involved in the Study

The compounds investigated in this study were provided by research groups worldwide with expertise in PDT. The set includes a diverse array of structurally distinct Pcs, which demonstrated notable activity, as reported in the original publications. In this study, we did not consider the use of any drug delivery system, carriers or conjugation with targeting moieties or the formation of nanoscale structures (which may change solubility, aggregation, targeting, etc.)[4−7] but focused only on compounds that are directly applied to cells. Several factors were considered for the selection of compounds in this study (Figure 1).

Hydrophilicity is a crucial property since a biological application is intended. Thus, compounds are decorated with charged (i.e., anionic (**A-series**), cationic (**C-series**)) or neutral polar (**N-series**) substituents to achieve sufficient water solubility. Among anionic derivatives, compounds carry either COO^- (**A1-A5Zn**) or SO_3^- (**A6-A8Zn**, **A9H**, and **A10Al**) functions. Quaternized nitrogen is present in all of the compounds of the cationic series (**C1-C14Zn**), except **C15Zn**, which contains aliphatic NH_2 groups. This group is believed to be protonated under physiological conditions.[8] Therefore, it has been classified as a cationic derivative as well. The neutral polar substituents come from either short PEG chains (**N1Zn**, **N3Zn**, **N6Zn**, **N7Zn**, and **N11Zn**), aliphatic alcohols (**N2Mg**), or carbohydrate moieties (**N4Zn**, **N5Zn**, **N8Zn**, and **N9Zn**). Additionally, **N10Zn** with ketal-protected glycerol moieties (potentially producing diols after acid-induced cleavage in lysosomes) has also been classified as neutral polar.

Compounds in all series also differ in the number and nature of polar groups and, consequently, in log P values. Finally, symmetrical hydrophilic derivatives (**A3-A8Zn**, **C5-C14Zn**, and **N6-N11Zn**) as well as unsymmetrical derivatives (**A1-A2Zn**, **C1-C4Zn**, **C15Zn**, **N1Zn**, and **N2Mg**) that are often amphiphilic were included in the study. Amphiphilic character usually favors effective interactions with biomembranes, which can result in changes in the PDT effect.[9,10] On the other hand, hydrophilic symmetric derivatives may benefit from better monomerization and water solubility. Direct comparison of unsymmetrical and symmetrical hydrophilic derivatives can therefore be very useful.

Aza analogs in which benzene rings are replaced for pyrazines (i.e., tetrapyrazinoporphyrazines) in **A5Zn** and **N7Zn**, as well as for pyridines (i.e., tetra(3,4-pyrido)-porphyrazines) in **C11Zn**, were included to determine the effect of the type of macrocyclic core.

The central metal plays a significant role in the production of singlet oxygen on the basis of the heavy atom effect.[11−14]

https://doi.org/10.1021/acs.jmedchem.5c03090
J. Med. Chem. 2026, 69, 4391−4407

Most of the derivatives in the study have a zinc(II) center, which is obvious from the code of the respective compounds (e.g., **A1Zn**, **C1Zn**, etc.). There are several exceptions to compounds having magnesium(II) (**N2Mg**), aluminum(III) (**A10Al**). and a metal-free form (**A9H**). Other central metals were not investigated in this study, but a recent study also proved that PtPc was a very efficient PS.[15]

Silicon(IV) Pcs constitute a distinct subgroup of compounds (**Si series**), because of the semimetal character of silicon and the important structural features this atom provides. Unlike other complexes, SiPcs allow for axial modification, which can reduce aggregation. The compounds of this subgroup are labeled as **SiX-C** or **SiX-N** in which the letter X denotes the compound number and C or N indicates the presence of a cationic or neutral axial ligand, respectively.

Clinically approved PSs[16] such as **protoporhyrin IX** (**PpIX**, the metabolic product of the 5-aminolevulinic acid (ALA) prodrug), **verteporfin**, **temoporfin**, and **Photosens** (i.e., **A10Al**) were used for comparison.

The synthetic procedures and details of the characterization of all the compounds involved in the study can be found in the original publications in the references listed in Table 1. In the following text, the physicochemical and photophysical properties are first described, followed by an evaluation of the photodynamic activity *in vitro* with attempts to correlate the efficacy with several structural parameters. All the experiments, if not otherwise stated, were performed under the same conditions in the same laboratory to avoid variability in the experimental conditions.

Spectral Properties

Since the effect of PDT is based on the activation of the PS by light, spectral properties represent important parameters that may respond to the environment. Detailed spectral studies were therefore carried out in DMF, where the vast majority of the compounds are monomeric, as well as in aqueous media (phosphate-buffered saline (PBS) and water), where the compounds can be partially or fully aggregated. Aggregation is undesirable in PDT because it leads to energy dissipation predominantly through internal conversion, thereby reducing or even completely inhibiting singlet oxygen production. Whereas a steep narrow Q-band is typical for monomeric species, aggregation is normally manifested by the broadening of the Q-band and the appearance of a new blueshifted band corresponding to H-aggregates (see spectra of representative examples in Figure 2 and the Supporting Information for all compounds).

Owing to the Pc core, most compounds of the series exhibit strong absorption with a low-energy Q-band between 660 and 710 nm and extinction coefficients between 150 and 300 000 M^{-1} cm^{-1} in DMF (Table 1). The position and shape of the Q-band are related to the type of core, the position of the substituents, and the central atom. Owing to the C_4-symmetry of the macrocycle, the Q bands of all the symmetrical compounds of the series in DMF were nonsplit (Figure 2a). In the case of unsymmetrical derivatives, both split and nonsplit Q bands were observed, which were dependent on the characteristics of the substituents. If the substituents do not have a strong electron-donating or electron-withdrawing effect or if they have a comparable effect, then splitting is usually not observed, even if the macrocycle has low symmetry. For example, splitting is significant at **C1Zn** (Figure 2e, black line) but less pronounced at **C2Zn**. Nonsplit Q bands are present in the spectra of **C3Zn**, **C4Zn**, and most of the other low-symmetrical Pcs of the series (Figure 2c, black line). Significant splitting can be observed in the case of metal-free **A9H**, again as a result of the loss of symmetry due to the presence of two central hydrogens instead of a metal ion. Notably, the splitting of **A10Al** in DMF is probably caused by an inconsistent sample composition due to the variable number of SO_3H groups, and splitting disappeared in aqueous media, where a nonsplit Q-band was present.

In terms of the position of the Q-band, compared to the corresponding Pc analogues **A4Zn** and **N6Zn**, the pyrazine analogs **A5Zn** and **N7Zn** exhibit well-known blueshifts of 52 and 35 nm, respectively.[37] On the other hand, significant redshifts can be achieved by shifting the substituents from peripheral (β positions) to nonperipheral positions (α positions),[38] which is reflected by the difference of 53 nm between the Q bands of **C9Zn** (eight α, 757 nm) and **C8Zn** (eight β, 704 nm). Similarly, a redshift of approximately 20 nm can be seen in **N9-N11Zn** (four α, ∼700 nm) compared with the structurally similar **N6Zn** and **N8Zn** derivatives (both four β, ∼680 nm).

Hydrophilicity

Because these compounds are intended for biological applications, studying their behavior in an aqueous environment is necessary. The Pc core is inherently highly hydrophobic and prone to $\pi-\pi$ stacking, but the hydrophilicity of the whole molecule can be modulated to a variable degree through the appropriate substituents. These modifications significantly influence their water solubility as well as their behavior in biological systems (e.g., membrane permeability, interaction with biomolecules, distribution). To examine the effects of various hydrophilizing groups, the partition coefficients between octanol and PBS (log *P*) were determined for the entire series (Table 1). It is evident that a highly hydrophilic character with log *P* values <−2.0, guaranteeing excellent water solubility, can be achieved by all types of peripheral substituents—anionic (**A1-A8Zn**), cationic (**C5-C7Zn**, **C10-C15Zn**), and neutral (**N6Zn**, **N8-9Zn**). The strongest effect on the hydrophilic properties is, however, through the introduction of anionic groups. It was clear from the comparison of unsymmetrical derivatives: anionic derivatives **A1-A2Zn** with the same number of hydrophilic groups exhibited log *P* values that were significantly lower than those of cationic **C3-C4Zn** with the same number of charged substituents, neutral hydrophilic PEGs (**N3Zn**), or carbohydrate (**N4Zn**) moieties. Interestingly, increasing the number of charges in the molecule is not the key to ensuring the high hydrophilicity of the molecule; already with 4 anionic charges (e.g., **A1-A2Zn**), a log *P* of ∼−2.5 can be achieved, whereas 16 such charges (**A3-A5Zn**) lead to only a slight reduction to a value of log $P \sim -3.0$. With respect to the Si(IV)Pcs series, **Si1-Si5** are lipophilic derivatives that are characterized by log *P* values greater than 0; therefore, the use of stock solutions in DMF or DMSO (instead of water) was required for spectral studies in aqueous media or *in vitro* tests (for details, see the Supporting Information).

Aggregation

The aggregation of various PSs in PDT is generally an unwanted property, as it decreases the activity of Pcs by the aggregation-caused quenching (ACQ) of the excited states. On the other hand, the aggregation of Pcs can also be beneficial, as it may introduce specific properties to the resulting aggregates

https://doi.org/10.1021/acs.jmedchem.5c03090
J. Med. Chem. 2026, 69, 4391−4407

leading to emerging applications[39] such as conversion to efficient type I PSs[40,41] or PSs for sonodynamic therapy,[42] photothermal therapy,[43] photoacoustic imaging,[44] or even uncommon phenomena, such as an aggregation-enhanced photodynamic effect.[45] In this work, we focused on the factors leading to a decrease in aggregation and ACQ.

In terms of the degree of aggregation in general, it appears that some of the structural factors promoting monomerization in water are specific to a certain type of compound (A, C, or N series), while others are generally applicable to all types of Pcs. For example, rigid bulky substituents with properly oriented (perpendicular to the macrocyclic ring) polar groups seem to be the universal key tool for all types of Pcs. The polar groups are then forced to be placed above and below the core, thus shielding the lipophilic core from water and maintaining the monomeric state. For the N-series, this is the only possibility evidenced by the fact that only **N6-N8Zn** ($8 \times \beta$) or **N9Zn** ($4 \times \alpha$) showed a sharp Q-band in water. In the case of anionic derivatives, the presence of 16 charged groups on the periphery (i.e., **A3-A5Zn**) ensured monomerization in aqueous media on the basis of strong repulsive forces. Anionic compounds with 4 or fewer anionic groups showed characteristic features of aggregation. Similar trends were observed in cationic derivatives, where 16 quaternized nitrogens in **C12-C14Zn** also enabled full monomerization. However, the C-series clearly revealed that, if the molecule is properly designed, even fewer charges can be sufficient for full monomerization. The key structural feature proved to be the rigidity of the peripheral arrangement, such that the polar groups cannot bend out and displace from their shielding position. Eight quaternized nitrogens on a flexible aliphatic linker did not sufficiently suppress aggregation (**C6Zn**, **C8Zn**, and **C9Zn**), whereas eight quaternized methylpyridine units incorporated into rigid aryloxy substituents led to complete monomerization (**C7Zn**). Additionally, **C11Zn** achieves full monomerization by combining the rigidity of the arrangement with the introduction of a substituent into sterically more demanding nonperipheral (α-) positions and the introduction of an additional charge into the core itself. Notably, compared with peripheral substituents, all types of Si(IV)Pcs (**Si1-Si5**) are advantageous because their axial ligands reduce the level of aggregation more efficiently. However, full monomerization in aqueous solutions was achieved only by those containing axial amino groups (**Si1-Si4**) that are basic and ionized in aqueous solutions (particularly in deionized water, which is more acidic than the physiological pH of 7.4 in PBS).

However, the conclusions from the aggregation must be interpreted very carefully. The biological environment is very complex, and interactions with various components, such as lipids, biomembranes, or proteins, may induce monomerization, as shown below in the example of interactions with bovine serum albumin (BSA). For this reason, the level of aggregation cannot be considered separately.

Photophysical Properties

The potential of the studied compounds to be good photosensitizers was first studied in solution, where the basic photophysical parameters, i.e., the quantum yield of singlet oxygen production (Φ_Δ), quantum yield of fluorescence (Φ_F), and fluorescence lifetime (τ_F), were determined. Because even partial aggregation would bias the measured values, which could lead to misinterpretation of structure−activity relationships, experiments were performed in DMF, thus ensuring monomerization of the involved Pcs (see above). Comparative methods using unsubstituted zinc(II) Pc as a reference (Φ_Δ = 0.56 in DMF,[46] Φ_F = 0.32 in THF[47]) or Rose Bengal (Φ_Δ = 0.47 in DMF; for porphyrin derivatives only)[48] were employed. The experimental details can be found in the Supporting Information.

The fluorescence emission spectra in both DMF and water were mirror images of particular absorption spectra (Figure 2b,d,f) with Stokes shifts of approximately 10 nm, which is a typical value for Pcs and related macrocycles.[49,50] In PBS and water, however, the fluorescence signal was often weaker when aggregation occurred (see Figure 2b, red line).

Most of compounds exhibit high singlet oxygen production ($\Phi_\Delta \sim 0.50-0.60$) while retaining reasonable fluorescence emission ($\Phi_F \sim 0.20-0.30$). This is true for anionic derivatives with $-SO_3H$ groups (**A6-A8Zn**), all compounds from the N-series (**N1-N11**), and all cationic derivatives **C1-C15Zn** (except **C6Zn**, which suffers from partial aggregation in DMF). Both Φ_Δ and Φ_F substantially decreased in anionic **A1-A5Zn** bearing COONa, which was caused by solubility issues associated with these derivatives in DMF. Similar problems were faced before,[17] and the quantum yields had to be determined for the corresponding free acids, which reached values comparable to those observed for most of the PSs in this study (e.g., Φ_Δ = 0.42 and 0.45; Φ_F = 0.19 and 0.12 for **A3Zn(COOH)** and **A4Zn(COOH)**, respectively).[17]

The heavy atom effect[12] is obvious because, compared with metal free **A9H**, magnesium **N2Mg**, and Al(III) **A10Al**, zinc derivatives generally have higher quantum yields. On the other hand, the latter two have higher fluorescence emission. Notably, the counteranion seems to have no effect on Φ_Δ and Φ_F if complete monomerization is ensured. Thus, fully monomeric **C5Zn-I** and **C5Zn-PF_6** have identical photophysical parameters ($\Phi_F \sim 0.27$, $\Phi_\Delta \sim 0.47$), whereas **C5Zn-SO_4** tends to aggregate (see comparison in Figure S44), leading to a significant decrease in values (Φ_F = 0.077, Φ_Δ = 0.28).

The Φ_Δ and Φ_F values of Si(IV)Pcs **Si1-Si5** were substantially lower despite being fully monomeric. For **Si5-N**, the reason is not entirely clear; in the case of **Si1-Si4** containing aliphatic amines, it is probably due to quenching of excited states via photoinduced electron transfer (PET) from the axial nitrogens to the macrocycle, as described previously.[35] Consequently, PET leads to decreasing values of Φ_Δ = 0.005−0.23 and Φ_F = 0.055−0.25 only. Under physiological conditions, these nitrogens are protonated, restoring efficient singlet oxygen production and fluorescence emission as also demonstrated previously.[35]

The trends in the values of the fluorescence lifetimes (τ_F) (see Table 1) correlated well with the values of Φ_F discussed above. The compounds with the highest Φ_F have τ_F of ∼3 ns, and the higher the Φ_F, the greater is the τ_F. If the quenching process occurred (PET or aggregation caused by solvent effects), biexponential decay with an additional fast component of τ_F < 1 ns was typically present.

In general, many of the studied Pcs had greater singlet oxygen production than the only clinically approved Pc for PDT (i.e., **Photosens**, $\Phi_{\Delta(DMF)}$ = 0.25, $\Phi_{F(DMF)}$ = 0.62), but they had comparable or slightly lower Φ_Δ values than those of clinically approved porphyrins: **PpIX**, **verteporfin**, and **temoporfin** exhibited high singlet oxygen production ($\Phi_{\Delta(DMF)}$ = 0.73−0.76, $\Phi_{\Delta(EtOH)}$ = 0.51−0.67) because of slightly decreased fluorescence emission ($\Phi_{F(DMF)}$ = 0.12−

https://doi.org/10.1021/acs.jmedchem.5c03090
J. Med. Chem. 2026, 69, 4391−4407

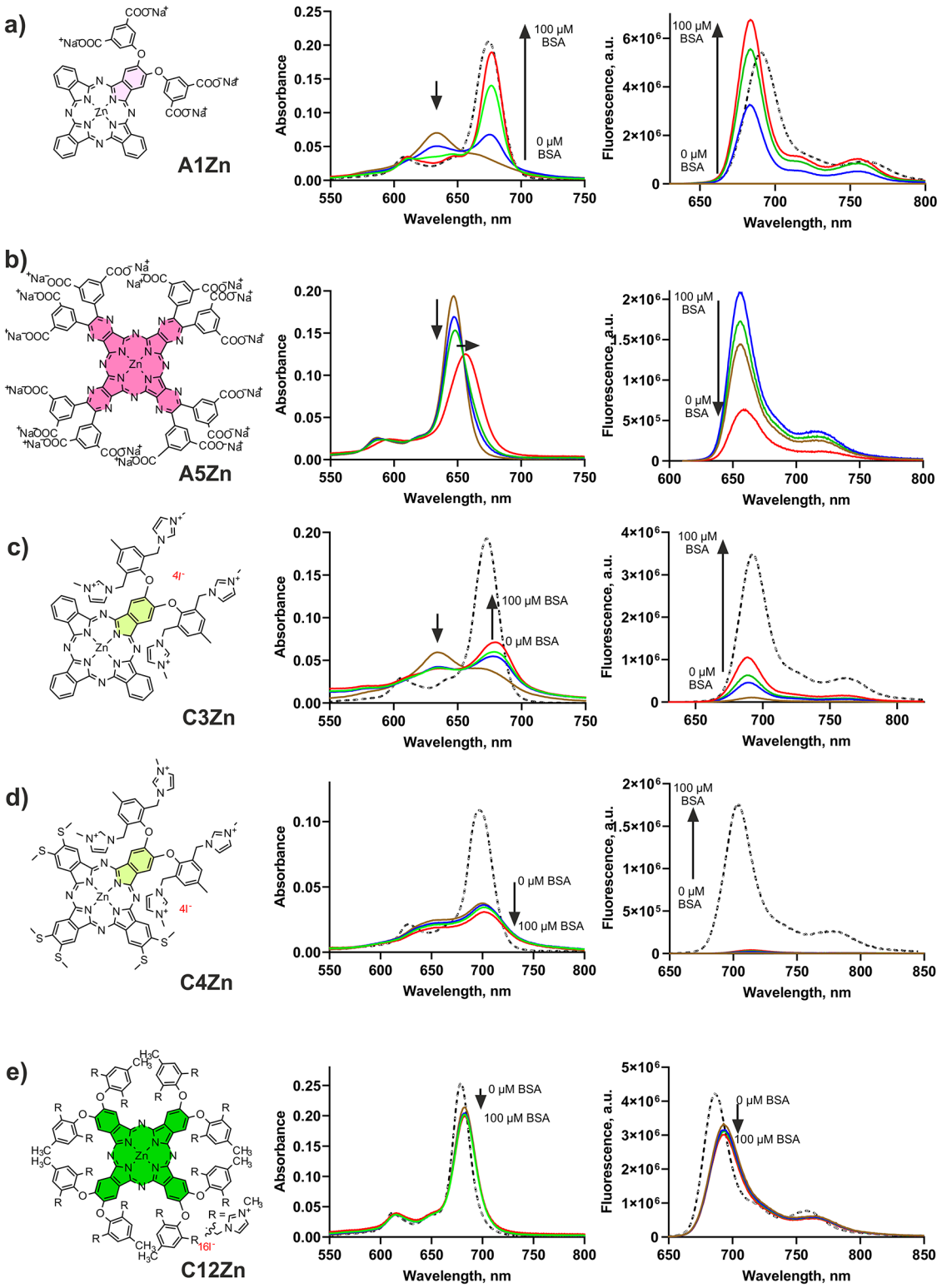

Figure 3. Representative examples of changes in absorption and fluorescence emission spectra upon interaction with BSA. Spectra of 1 μM Pc in PBS (brown line) were taken, and then, BSA was added to attain final concentrations of 17.5 μM (blue line), 35 μM (green line), and 100 μM (red line) in a cuvette. For comparison, spectra in monomeric state (DMSO (a), DMF (c–e)) are added as dashed black lines. Compound **A5Zn** is not well soluble in organic solvent but monomeric already in PBS. Spectra of all compounds of the series are shown in Supporting Information Figures S45–S87.

0.24). Despite this, Pcs are a promising group of PSs because of their much stronger absorption (ε typically an order of magnitude higher than that of porphyrins) in the optical window of biological tissues, which enables the use of lower light or drug doses for efficient activation.

https://doi.org/10.1021/acs.jmedchem.5c03090
J. Med. Chem. 2026, 69, 4391–4407

Table 2. Photodynamic Activity of All Derivatives Assessed on HeLa (Human Cervical Carcinoma), MCF-7 (Human Lung Carcinoma), and SK-MEL-28 (Human Skin Melanoma) Cell Lines

Cpd.	EC_{50} (nM) HeLa	Ref[a]	EC_{50} (nM) MCF-7	Ref[a]	EC_{50} (nM) SK-MEL-28	Ref[a]	Subcellular localization (HeLa)	Ref[a]
A1Zn	290 ± 78	17	453 ± 26	17	530 ± 30	t.w.	Ly, Me	t.w.
A2Zn	410 ± 156	17	584 ± 88	17	700 ± 50	t.w.	Ly, Me	t.w.
A3Zn	5160 ± 1030	17	3470 ± 670	17	2000 ± 300	t.w.	Ly	t.w.
A4Zn	10 310 ± 1020	17	5090 ± 1240	17	12 700 ± 2400	t.w.	Ly[17]	t.w.
A5Zn	5700 ± 1100	54	3010 ± 740	17	10 800 ± 2100	t.w.	Ly[54]	t.w.
A6Zn	12 000 ± 3000	t.w.	22 100 ± 6600	t.w.	10 400 ± 3600	t.w.	Ly	t.w.
A7Zn	1300 ± 400	t.w.	5100 ± 350	t.w.	2120 ± 560	t.w.	Ly	t.w.
A8Zn	1000 ± 300	t.w.	2470 ± 810	t.w.	1200 ± 280	t.w.	Ly	t.w.
A9H	85 ± 7	t.w.	347 ± 125	t.w.	300 ± 77	t.w.	Ly, Me	t.w.
A10Al	2070 ± 290	55	2040 ± 310	17	1900 ± 200	t.w.	Ly	t.w.
C1Zn	27 ± 9	17	35 ± 2	17	22 ± 3	t.w.	Ly, Me	17
C2Zn	105 ± 34	10	65 ± 8	10	62 ± 11	t.w.	Ly, Me	10
C3Zn	48 ± 19	17	21 ± 8	17	40 ± 4	t.w.	Ly, Me	17
C4Zn	79 ± 20	10	61 ± 9	10	108 ± 24	t.w.	Ly, Me	10
C5Zn-I	62 ± 13	t.w.	60 ± 10	t.w.	110 ± 10	t.w.	Ly	t.w.
C5Zn-PF_6	52 ± 26	t.w.	100 ± 20	t.w.	190 ± 40	t.w.	Ly	t.w.
C5Zn-SO_4	53 ± 9	t.w.	80 ± 30	t.w.	150 ± 50	t.w.	Ly	t.w.
C6Zn	58 ± 20	t.w.	110 ± 30	t.w.	150 ± 50	t.w.	Ly	t.w.
C7Zn	480 ± 250	24	50 ± 14	24	1880 ± 370	t.w.	Ly	24
C8Zn	540 ± 90	25	280 ± 40	t.w.	320 ± 48	25	Ly	t.w.
C9Zn	310 ± 121	25	210 ± 10	t.w.	220 ± 21	25	Ly	25
C10Zn	148 ± 45	t.w.	186 ± 76	t.w.	524 ± 152	t.w.	Ly	t.w.
C11Zn	3.8 ± 0.2	55	2.8 ± 0.1	55	3.8 ± 0.6	55	Ly	55
C12Zn	37 ± 6	26	11 ± 3	17	45 ± 7	t.w.	Ly	26
C13Zn	12 ± 4	27	5.3 ± 0.8	27	56 ± 6	t.w.	Ly	27
C14Zn	110 ± 27	24	47 ± 16	24	64 ± 2	t.w.	Ly	24
C15Zn	74 ± 22	t.w.	50 ± 8	t.w.	25 ± 6	t.w.	Ly	t.w.
N1Zn	17 ± 5	t.w.	6 ± 1	t.w.	16 ± 3	t.w.	Mi	t.w.
N2Mg	107 ± 1	t.w.	190 ± 40	t.w.	119 ± 14	t.w.	Ly	t.w.
N3Zn	2200 ± 160	30	1500 ± 300	30	900 ± 200	30	Ly	t.w.
N4Zn	2070 ± 60	30	1200 ± 100	30	500 ± 100	30	Ly	t.w.
N5Zn	4970 ± 930	30	2400 ± 300	30	1030 ± 160[30]	t.w.	Ly	30
N6Zn	69 700 ± 10 700	30	233 000 ± 6000	t.w.	305 000 ± 29 000	t.w.	Ly	t.w.
N7Zn	75 700 ± 17 100	30	228 000 ± 9000	t.w.	306 000 ± 46 000	t.w.	Ly	t.w.
N8Zn	354 000 ± 42 000	32	287 000 ± 47 000	t.w.	183 000 ± 44 000	t.w.	Ly	t.w.
N9Zn	163 000 ± 66 000	32	170 000 ± 23 000	t.w.	189 000 ± 34 000	t.w.	Ly	t.w.
N10Zn	540 ± 80	t.w.	430 ± 60	t.w.	360 ± 50	t.w.	Ly	t.w.
N11Zn	560 ± 80	t.w.	31 ± 12	t.w.	45 ± 3	t.w.	Ly	t.w.
Si1-C	49.2 ± 26.0	t.w.	11 ± 4	t.w.	11 ± 3	t.w.	Ly	t.w.
Si2-C	80 ± 30	t.w.	54 ± 7	t.w.	49 ± 6	t.w.	Ly	t.w.
Si3-C	10 ± 3	t.w.	13 ± 4	t.w.	11 ± 3	t.w.	Ly, Mi	t.w.
Si4-C	2.7 ± 0.6	t.w.	5.5 ± 1.3	t.w.	7.5 ± 1.1	t.w.	Ly	t.w.
Si5-N	2.5 ± 0.3	t.w.	9.2 ± 2.4	t.w.	6.6 ± 1.1	t.w.	Mi	t.w.
PpIX	5500 ± 600	t.w.	5700 ± 800	t.w.	6200 ± 300	t.w.		
verteporfin	36 ± 10	55	33 ± 3	t.w.	21 ± 3	t.w.		
temoporfin	45 ± 7	55	210 ± 74	t.w.	103 ± 17	t.w.		

[a]The data with literature references have been determined previously under the same experimental conditions at the same workplace and published. t.w. = this work. Cells were incubated with the compounds for 12 h, washed, and subsequently irradiated with a Xe-lamp for 15 min (λ > 570 nm, 11.2 J/cm^2). Results are expressed as mean ± SD. Ly, lysosomes; Me, membrane; Mi, mitochondria. EC_{50} values are reported in the same range (nM) for easy comparison of photodynamic activities among all compounds. For values using only significant figures, please see Figures S88–S93.

Interaction with BSA

To obtain deeper insight into biologically relevant media, the interaction of the compounds with serum proteins were investigated since serum proteins play important roles in the biodistribution of drugs, affecting their distribution, efficacy, and elimination. Albumin, which is the most abundant one, is well-known to strongly bind anionic drugs, mainly into the positively charged binding sites formed predominantly by basic amino acid residues (Lys, Arg, and His).[51] This finding is in accordance with several records in the literature, which show that anionic Pcs strongly bind to BSA[17] or aid in the specific disassembly of anionic Pc nanostructures.[52] The amount of BSA was chosen to mimic the typical concentration of BSA in

https://doi.org/10.1021/acs.jmedchem.5c03090
J. Med. Chem. 2026, 69, 4391−4407

serum-containing medium (35 μM), half of that amount (17.5 μM), and an excess (100 μM).

Spectral studies performed in PBS with different amounts of BSA (Figures S46−S89) revealed that almost all types of derivatives were affected by BSA in some way. In the case of the aggregated compounds of the A-series, the addition of BSA aided in the partial (**A2Zn**, **A6Zn**, and **A9H**) or complete (**A1Zn**, **A7Zn**, and **A8Zn**) disaggregation of the compounds into monomerized compounds, which was also obvious from increased fluorescence emission (Figure 3a). The addition of BSA to nonaggregating derivatives (**A3Zn**, **A4Zn**, **A5Zn**, **A10Al**) led to a slight bathochromic shift in the Q-band accompanied by partial quenching of the excited states, which was observed as a decrease in the Q-band maximum and fluorescence intensity (Figure 3b), which was negligible in the case of Pcs (**A3Zn**, **A4Zn**, and **A10Al**) but significant in the case of the aza analog **A5Zn**. Thus, although interaction with BSA increases the monomeric level of anionic Pcs, it can lead to quenching of the excited states of some of them (in particular, AzaPcs), which in turn can worsen the final photophysical properties, as has been shown for symmetric monomeric substances.

Different behaviors were observed in the C-series, where complete monomerization was not observed for any of the aggregated derivatives, indicating rather limited interactions with BSA. Partial monomerization evident from changes in the absorption spectra and an increase in fluorescence emission occurred in the case of strongly aggregated low-symmetrical **C1Zn**, **C3Zn**, and **C15Zn** (Figure 3c). In the case of less aggregated derivatives (**C4Zn**, **C5Zn**, and **C8Zn**), the interaction of BSA led to a slight decrease in the absorption band (without a shift in the spectrum) but was accompanied by a slight increase in the fluorescence intensity (Figure 3d), which indicates a probable effect of monomerization. Nevertheless, the level of monomerization was rather low for the C-series. These findings are in agreement with recent publication on the interactions of a series of cationic Pcs with different numbers of cationic functions with BSA, where rather limited spectral changes were observed even at high (200 μM) concentrations of BSA.[53] Finally, the absorption and fluorescence emission spectra of monomeric derivatives of the C-series (**C7Zn**, **C9Zn**, and **C11Zn-C14Zn**) were almost unaffected (Figure 3e), which proves that, in contrast to anionic derivatives, cationic derivatives do not bind significantly with BSA.

Similarly to the C-series, the ability of BSA to monomerize aggregated Pcs was also evident in the N-series, where the fluorescence was slightly enhanced for the strongly aggregated compounds **N2Mg**, **N10Zn**, and **N11Zn**, although no changes were observed in their absorption spectra. In the case of less aggregated **N1Zn** and **N3-N5Zn**, monomerization was apparent even from the absorption spectra, again with a significant increase in the monomeric form documented by the increase in the fluorescence intensity. The addition of BSA to the monomeric **N6-N9Zn** derivatives resulted in no change in spectral properties, similar to those observed for monomeric cationic species, demonstrating that the interaction of uncharged Pcs with BSA did not occur.

Owing to the monomeric character of the Si-series, their interactions with BSA correspond to those of the above-mentioned derivatives in the fully monomeric state. Thus, the absorption spectra of cationic Si(IV)Pcs were not affected by the presence of BSA; only in the case of **Si3-C** was a decrease in the Q-band accompanied by fluorescence quenching. On the other hand, the addition of BSA to aggregated **Si5-N** enhanced fluorescence emission, while the absorption spectra remained unchanged, again indicating rather limited interaction.

In summary, interactions with BSA seem to be important, particularly for the A-series. It may quench the excited states of some PSs (which is rather an exception) but simultaneously aid in the monomerization of aggregated species, thus increasing the number of photoactive species. Therefore, even aggregated PSs may become active in biological environments. Notably, the attachment of Pcs to proteins may, however, result in strong chemical quenching of produced singlet oxygen by its reaction with susceptible amino acids in BSA as the closest target.[17] These crucial cytotoxic species may not be amenable to the destruction of other biomolecules in cells. Once the Pcs are attached to the BSA, they are taken up by cells through endocytosis in this complex.

In Vitro Studies

The photophysical properties and spectral analysis of Pcs provide useful insights for predicting photodynamic activity; however, such parameters are not always fully predictive, because of the complexity of the biological environment. Additional factors—including cellular uptake and localization, interactions with serum proteins and biomembranes, and variations in pH across different cellular compartments—can substantially influence biological outcomes. To account for these variables, all of the Pcs examined in this study were subjected to biological evaluation to better define the structural features relevant to PDT activity.

Detailed *in vitro* studies involving subcellular localization and determination of the EC_{50} in three different cell lines (human cervical carcinoma—HeLa, human breast adenocarcinoma—MCF-7, and human skin melanoma—SK-MEL-28) were performed. A broadband light source (ozone-free 450 W Xe-lamp, Newport) equipped with the long-pass filter Schott OG570 was used (12.4 mW/cm^2, 15 min, 11.2 J/cm^2). This setup provided a stable irradiance between 600 and 800 nm (see Figure S129), thereby minimizing variability in the activation of different Pcs and enabling reliable comparison of results across compounds. The *in vitro* findings are summarized in Table 2 and Figures 4−6 and S88−S128.

Initial analysis was performed by using HeLa cells, although the observations are generally applicable to the other cell lines examined. The results revealed an extremely wide range of photodynamic activity with EC_{50} (HeLa) ranging from 2.5 nM to 354 μM with no consistent correlation with the determined Φ_Δ (Figure 5a). For example, the symmetrical derivative **A4Zn** was monomeric in water and strongly produced singlet oxygen in DMF (Φ_Δ = 0.45) but had relatively low photodynamic activity (EC_{50} = 10.31 μM, HeLa cells). In contrast, structurally related unsymmetrical **A2Zn** with an identical peripheral group reached 25× higher photodynamic activity under identical conditions (EC_{50} = 0.41 μM) despite being aggregated in water and having half the value of Φ_Δ in DMF (Φ_Δ = 0.22). Direct correlations of the EC_{50} values with the Φ_Δ or log *P* parameters (Figure 5) did not yield clear structure−activity relationships. The only consistent trend was the enhanced photodynamic activity observed for the N-series with increasing lipophilicity (Figure 5b, blue). These findings highlight the necessity of a broader, multifactorial interpretation of the results.

https://doi.org/10.1021/acs.jmedchem.5c03090
J. Med. Chem. 2026, 69, 4391−4407

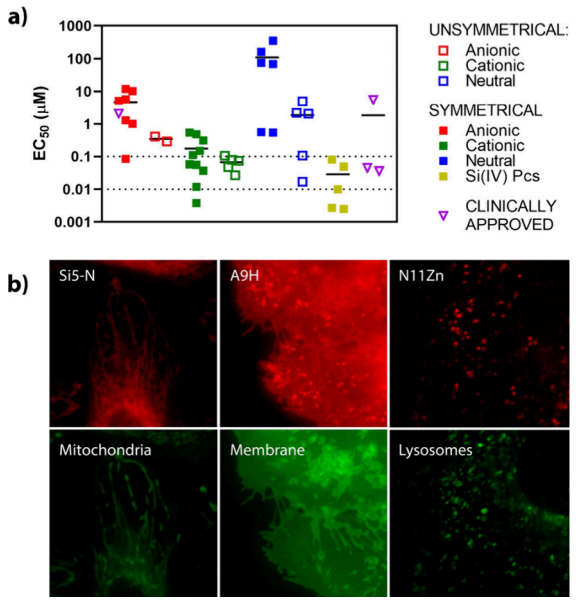

Figure 4. *In vitro* experiments on HeLa cells: (a) depiction of EC_{50} values of all studied compounds grouped by their structural characteristics (charge, position of substituents); silicon derivatives represent separate groups (analogical data for MCF-7 and SK-MEL-28 cell lines can be found in Supporting Information Figure S122). Compound **A10Al** (Photosens) is included in the "symmetrical anionic" group (red full squares) and marked as a purple open triangle (clinically approved); (b) subcellular localization of selected derivatives localizing into mitochondria (**Si5-N**), cytoplasmic membrane (**A9H**), and endolysosomal compartment (**N11Zn**); red—photosensitizer, green—organelle-specific probes.

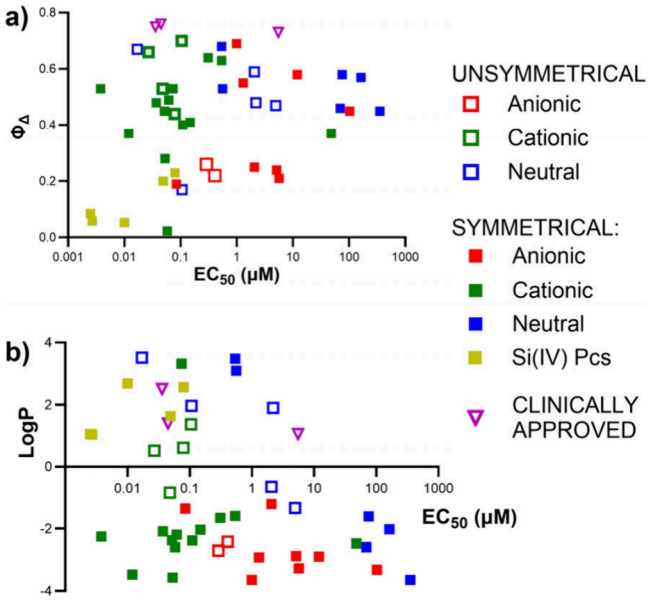

Figure 5. Correlation of EC_{50} (HeLa) with Φ_Δ (a) or log *P* (b) parameters.

For a long time, subcellular localization was deemed to be one of the critical factors of the resulting PDT effect.[56] This was largely attributed to the limited diffusion distance of singlet oxygen from its site of generation.[57] It has been repeatedly demonstrated that the localization of PSs within target cells influences not only the photodynamic activity but also the predominant type of cell death (together with the light dose).[58] Therefore, the subcellular localization of all the studied derivatives was assessed in the HeLa cell line (human cervical carcinoma), the most widely used model cell line.[59] Nearly all of the derivatives investigated in this study were predominantly localized in endolysosomal compartments (Figures 4b, S94–S97, S99–S105, and S107–S117) with several compounds also detected in additional organelles. Notably, **Si3-C** exhibited dual localization in both lysosomes and mitochondria (Figures 4b and S116). Moreover, compounds **Si5-N** (Figure S118) and **N1Zn** (Figure S106) were the only PSs that were not detected in lysosomes at all, indicating exclusive mitochondrial localization. Cytoplasmic membrane localization (in addition to that of lysosomes) was observed with some charged unsymmetrical Pcs (**A1Zn**, **A2Zn**, and **C1-C4Zn**) and low-symmetry **A9H** (Figures 4B and S98). Localization to adiposomes,[60] the Golgi apparatus,[61] nuclei,[62] or other organelles was not detected, unlike for some other PSs, PS-containing delivery systems, or PS containing targeting moieties reported in the literature.

Given that almost all of the derivatives were localized to lysosomes, subcellular localization can hardly be used as a parameter for predicting photodynamic activity, especially considering the wide range of EC_{50} values of derivatives localized in lysosomes, starting at 2.5 nM (**Si5-N**) and reaching values as high as 354 μM (**N8Zn**). Although PSs localizing to mitochondria are among the most active derivatives (**N1Zn**, **Si3-C**, and **Si6-N** with EC_{50} values of 17 nM, 10 nM, and 2.5 nM, respectively), this localization is not determining the high activity, as derivatives such as **Si4-C** (2.7 nM), **C11Zn** (3.8 nM), or **C13Zn** (12 nM) are solely localized to lysosomes but still retain comparable photodynamic activity upon irradiation.

With respect to peripherally decorated Pcs, most members of the **A-** and **N-series** are less active than those of the **C-series** compounds. The overall situation when the compounds are divided into subgroups (symmetrical, unsymmetrical, cationic, anionic, and neutral) is shown in Figure 4, and subsequent subanalyses of the specific situations (type of function and flexibility) are shown in detail in Figure 6 (including statistical analysis) and are described in the following paragraph.

The difference between the **C-series** and the other two series was statistically significant (Figure 6n,p), whereas the difference between the **A-series** and **N-series** was not significant (Figure 6o). For both **A-** (Figure 6a–c) and **N-series** (Figure 6j–l), symmetrical derivatives were generally less active than unsymmetrical derivatives, whereas the **C-series** compounds exhibited the opposite trend (Figure 6h); however, it was strongly dependent on whether the comparison is made with compounds with similar types of substituent (i.e., in a rigid or flexible arrangement (see below)). Notably, unlike the two other series, all of the anionic derivatives strongly interacted with BSA, which may explain their weaker effect. One of the literature studies also reported that much higher activity of anionic Pcs in vitro was observed when the cells were treated in serum-free medium, whereas no difference was observed in cationic derivatives.[17]

With respect to the **A-series**, amphiphilic anionic derivatives (**A1Zn** and **A2Zn**) were ~21 times more active than their symmetrical hydrophilic counterparts (**A3Zn** and **A4Zn**), which can be attributed to the preservation of the monomeric state because of the interaction of unsymmetrical derivatives with the membranes,[17] and this was also consistent when the whole series was analyzed (Figure 6a). Water-soluble symmetrical anionic derivatives may be negatively influenced by

https://doi.org/10.1021/acs.jmedchem.5c03090
J. Med. Chem. 2026, 69, 4391–4407

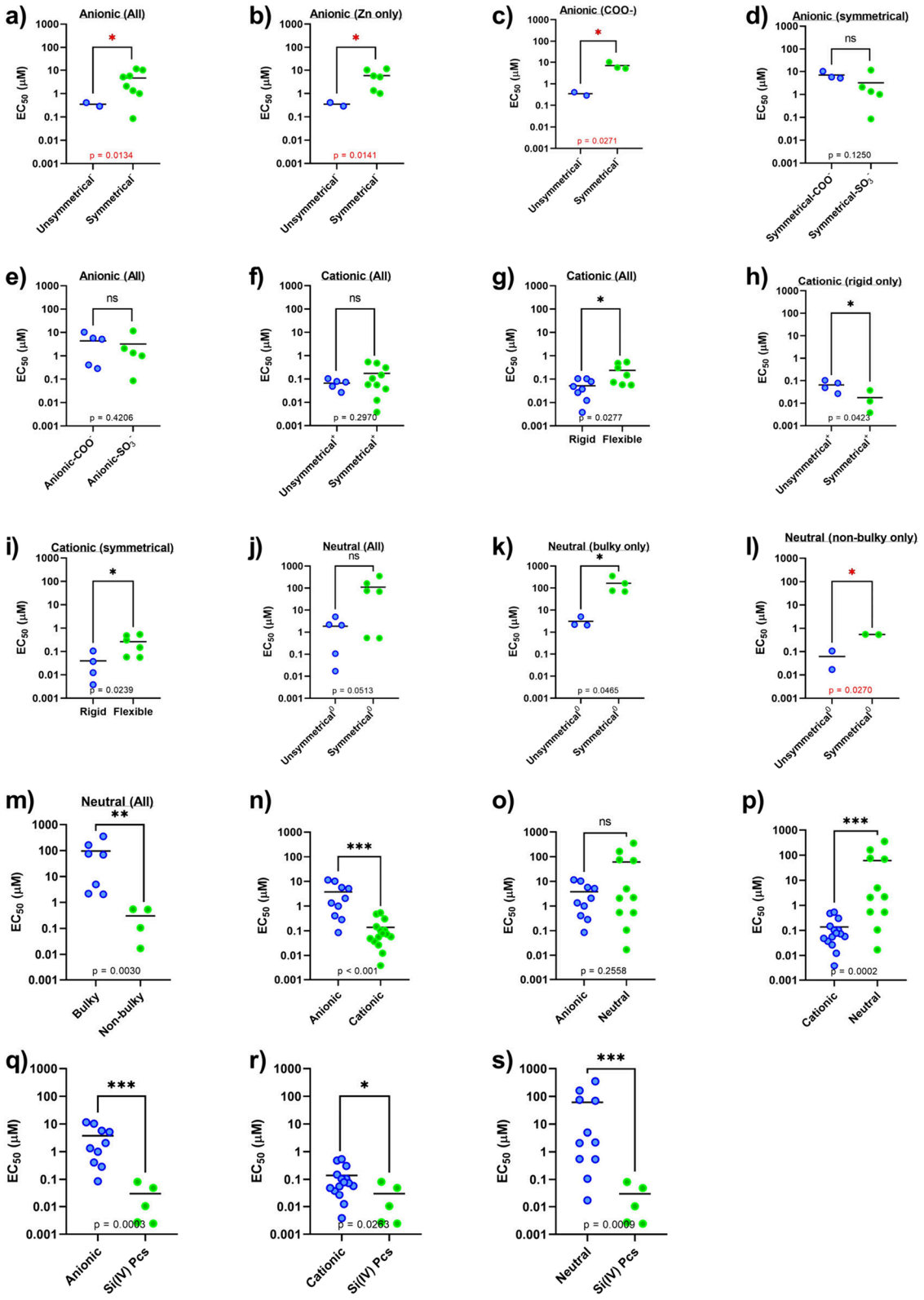

Figure 6. Comparison of the photodynamic activities of different groups of photosensitizers against HeLa cells. Analysis (*t* test) is marked red if at least one group contains only two members. (a–e) Anionic compounds, (f–i) cationic compounds, and (j–m) neutral compounds. (n–s) Comparison of all main groups. For a detailed description of the statistical analysis, see the Supporting Information.

low intralysosomal pH via charge neutralization and subsequent aggregation in this environment, as we previously demonstrated.[17] On the other hand, this does not have to be the only factor since no improvement was observed in those Pcs bearing more acidic sulfonate functions (Figure 6d,e).

In the **N-series**, the PDT activity correlated well with the lipophilicity expressed as log *P* (Figure 5b). An increase in

https://doi.org/10.1021/acs.jmedchem.5c03090
J. Med. Chem. 2026, 69, 4391−4407

activity was observed with less hydrophilic unsymmetrical analogs compared with their fully hydrophilic symmetrical analogs: **N3Zn** (2.20 μM), **N4Zn** (2.07 μM), and **N5Zn** (4.97 μM) versus **N6Zn** (69.71 μM) and **N8Zn** (354 μM) (Figure 6j–l). The bulkiness and high polarity of the substituents seem to play significant roles (Figure 6m), as they represent obstacles to efficient cellular uptake. It has also been independently reported in the literature recently that symmetrical derivatives of the **N-series** with lower activity had substantially lower cellular uptake than their unsymmetrical more lipophilic derivatives.[30,63,64] This is further supported by the highest photodynamic activity of unsymmetrical derivatives with nonbulky moieties **N1Zn** and **N2Mg** with EC_{50} values of 17 and 107 nM, respectively, which are significantly more lipophilic, with log $P \geq 2$. They are closely followed by symmetrical nonbulky derivatives **N10Zn** and **N11Zn**. Statistical analysis of the **N-series** containing either bulky or nonbulky moieties also revealed significant differences between unsymmetrical and symmetrical compounds (Figure 6k,l), which might be a consequence of the lower lipophilicity of the latter.

The activity of cationic derivatives (**C-series**) was among the highest in this investigation and was affected by two main structural characteristics: the bulkiness and rigidity of peripheral moieties (Figure 6g) and, as outlined above, the introduction of amphiphilic character. Moieties in cationic derivatives that are rather small (e.g., in **C8Zn** and **C9Zn**) are flexibly linked to the core, and their position relative to the core may change, leading to inefficient protection against aggregation in aqueous environments. Consequently, they were characterized by decreased activity in this series (EC_{50} = 540 and 310 nM, respectively; Figure S89). Compounds bearing more bulky moieties that are still flexible (e.g., **C5Zn-I**, **-PF_6**, and **-SO_4**) had lower EC_{50} values (62, 52, and 53 nM, respectively; Figure S89). However, derivatives with very bulky moieties in a rigid arrangement (e.g., **C11Zn** and **C13Zn**) do not enable repositioning of the charges relative to the core (therefore possessing great protection against aggregation) and represent very potent PSs with extremely low EC_{50} values (3.8 and 12 nM, respectively; Figure S90). Therefore, unlike the **N-series** (Figure 6m), increasing the bulkiness of the moieties increases the photodynamic activity of the **C-series** derivatives because of their rigid arrangement (Figure 6g). The second difference is in the behavior of the unsymmetrical analogs (Figure 6h), where the statistical analysis indicates better results for the symmetrical Pcs. In direct comparison, unsymmetrical cationic derivatives (e.g., **C1Zn** and **C2Zn**, one cationic moiety bearing 3 charges) were slightly less potent than their symmetrical counterparts (**C11Zn**, four cationic moieties bearing 12 charges in total). Similar results were also obtained from the comparison of unsymmetrical **C3Zn** and **C4Zn** (two cationic substituents with 4 charges in total) with symmetrical **C12Zn** analogs (eight cationic moieties with 16 charges in total). Notably, the activity of **C5Zn-I**, **-PF_6**, and **-SO_4** did not significantly differ; therefore, the influence of these counterions on the photodynamic activity is likely very low (Figure S119).

Silicon derivatives stand out from the whole series because they are not decorated with moieties on the periphery but contain axial substituents linked to the central Si(IV) atom (Figure 1). Owing to this feature, all Si(IV)Pcs are well protected against aggregation, leading to very efficient PSs with the best activities (with EC_{50} values ranging from 2.5 to 80 nM), which were significantly better than those of the **A-** or **N-series** and with comparable results to those of the whole **C-series** (Figure 6q,r,s) (Table 2, Figure S92).

In general, **C-series** and **Si-series** were more potent PSs than the **A-series** and **N-series**, and the **A-series** vs **N-series** did not significantly differ (Figure 6n–s).

Notably, all the above-mentioned results were obtained using the HeLa cell line, but two other malignant cell lines were used to further support the behavior of all the studied derivatives: the human breast carcinoma cell line MCF-7 and the human skin melanoma cell line SK-MEL-28. Comparisons between the effects of the analogs on these cell lines and statistical analyses revealed similar trends (Figures S120 and S121), which were sometimes even more pronounced: e.g., the increase in the activity of **C12Zn** in comparison with that of **C3Zn** was just 1.3× greater in HeLa cells but 2× and 12× greater in MCF-7 and SK-MEL-28 cells, respectively. However, overall, the EC_{50} values were comparable between the cell lines (Table 2, Figures S88–S93) with no significant difference when the whole series was considered (Figure S123), although for particular derivatives, small differences were observed (Figures S124–S128).

Notably, some of the clinically approved photosensitizers were included in this study: porphyrin-based PSs **verteporfin**, **temoporfin**, and **PpIX** (the active form of the prodrug δ-aminolaevulinic acid and its derivatives) and the above-mentioned **Photosens** (**A10Al**). While the photodynamic activity of **PpIX** (EC_{50} = 5.5 μM) was similar to that of anionic symmetrical analogs (including **A10Al**), **verteporfin** and **temoporfin** reached reasonably high photodynamic activity comparable, e.g., with some cationic derivatives with EC_{50} values of 36 nM and 45 nM, respectively (Table 2, Figures S88–S93). The activity of **Photosens** perfectly corresponded to the relationships derived for anionic symmetrical Pcs (see Figure 4a).

CONCLUSIONS

There are a number of factors that may affect the (photo)-toxicity and subsequent usability of any drug in treatment. This extensive study of different types of Pcs under the same experimental conditions enabled us to define some of the factors influencing the spectral, photophysical, and PDT properties. Compared with porphyrins and chlorins, which form a typical group of clinically approved PSs, Pcs absorb strongly in the Q-band area ($\varepsilon \sim 150–300\,000$ M^{-1} cm^{-1}), which is advantageous and may lead to a stronger PDT effect and a reduction in the dose of PS during cancer treatment. A significant red-shift of the Q-band can be achieved by the introduction of substituents to nonperipheral (α-) positions, which may further increase the therapeutic impact of PSs since red light penetrates deeper into tissues.

Owing to the planar macrocycles, the lipophilic *Pc* core tends to aggregate in aqueous medium. A comparison of the Pcs in this series clearly revealed that the most efficient way to achieve monomerization is to either use Si(IV)Pcs or introduce charged bulky groups into a rigid arrangement. Furthermore, aggregation may be partially suppressed by BSA present in biological media, especially in the case of anionic derivatives, whose strongest interactions are based on electrostatic interactions. The photophysical parameters of the monomeric forms of the studied Pcs (in DMF) were almost identical within the whole series with $\Phi_\Delta \sim 0.50–0.60$ and $\Phi_F \sim 0.20–0.30$, following well-known rules such as the heavy

https://doi.org/10.1021/acs.jmedchem.5c03090
J. Med. Chem. 2026, 69, 4391–4407

atom effect, higher Φ_Δ for nonperipherally substituted derivatives, and quenching by PET (in the case that an amine is present in the molecule).

There are no measurable in-solution parameters that can be used to simply predict PDT activity. More key structural factors must be combined to obtain effective PSs. Notably, this may change if carriers are used to transport the PSs. The use of carriers, supramolecular assemblies, and various drug delivery systems as alternative ways to modify different parameters of PSs, such as aggregation, cellular uptake, localization, and ROS generation at the site of action, was not the aim of this study. The key findings from this study can be summarized as follows:

- Cationic Pcs generally possess higher activity (lower EC_{50} values) than anionic and neutral Pcs probably because of limited binding to BSA and other factors described elsewhere.[17]
- Si(IV)Pcs are superior PSs in general because they effectively protect against aggregation because of axial substituents.
- Introduction of rigid bulky substituents to the periphery is the key tool to achieve full monomerization for all types of Pcs (anionic, cationic, or neutral). Bulkiness increases the PDT activity of cationic derivatives but decreases activity of neutral derivatives.
- Interaction with biomolecules (such as serum albumin) may help in monomerization but also partially quenches the excited states of some derivatives, particularly aza-analogues. Interaction with BSA also seems to be the cause for the lower activity of anionic Pcs.
- Low-symmetry character resulting in amphiphilic molecules substantially improves the activity of neutral and anionic derivatives but has rather limited effects on cationic derivatives.

On the basis of these observations, several recommendations for the design of Pcs for PDT can be proposed to maximize the effects. Axial substitution in SiPcs is favorable for modification, despite lower singlet oxygen production. In other metal complexes, the optimal strategy depends on the nature of the substituents. For neutral groups (e.g., PEG, sugars, and alcohols), smaller substituents are favored, maintaining high lipophilicity while retaining sufficient water solubility to enable cellular application. Cationic derivatives generally exhibit high photodynamic activity; to further enhance efficacy, bulky and rigid substituents positioned above and below the macrocyclic core are recommended with no clear requirement regarding symmetrical versus unsymmetrical substitution. In the case of anionic derivatives, unsymmetrical substitution, leading to amphiphilic structures, is preferable.

The results of this study provide a general framework for structural features that may influence *Pc*-mediated PDT activity *in vitro*. However, it remains challenging to consolidate these findings into a universal design principle, as multiple factors can contribute to the overall effect. Therefore, the conclusions presented here should be regarded as guiding considerations rather than definitive rules and are intended to serve as a basis for further critical evaluation in the design of new PSs.

EXPERIMENTAL SECTION

General

The UV/vis spectra were recorded on a Shimadzu UV-2600 spectrophotometer (Shimadzu, Kyoto, Japan). The fluorescence spectra were recorded on a FLS-1000 or FS-5 Photoluminescence Spectrometer (Edinburg Instruments, Edinburg, United Kingdom). Statement of purity: The present study utilized compounds that have been previously synthesized and characterized in peer-reviewed publications. As these compounds underwent prior analytical validation and their purity was verified during the original studies, additional purity testing was not repeated herein. The samples were employed as obtained from the cited sources under the assumption that their reported purity was adequate for the intended evaluations.

Sample Source

All of the compounds were obtained from the authors of their first publication. The synthesis and source of the compounds are mentioned Table 1.

Absorption and Emission Spectra

A 100 μM stock solution of the Pc was prepared in water (**A3Zn**, **A4Zn**, **A5Zn**, **A7Zn**, **C5**, and **C6Zn**), DMF/water 10:1 (**A1Zn**, **A2Zn**, and **C9Zn**), or DMF (all other samples of the series). An absorption spectrum of 2.475 mL of solvent (water, DMF, or PBS) was taken (i.e., absorption spectrum of baseline); then, 25 μL of stock solution was added to reach the final concentration of 1 μM in the cuvette, and the absorption and emission spectra were taken. Baseline of the solvent was subtracted from the obtained absorption spectrum to get the final absorption spectrum of the sample. The excitation wavelengths were as follows: 575 nm (**N7Zn**, **PpIX**), 600 nm (**A5Zn**, **verteporfin**, **temoporfin**), 605 nm (**C5Zn-I**, **C5Zn-PF$_6$**, **C5Zn-SO$_4$**, **C10Zn**, **Si1-C**, **Si2-C**), 610 nm (**A1Zn**, **A2Zn**, **A3Zn**, **A6Zn**, **C1Zn**, **C3Zn**, **C12Zn**, **C13Zn**, **C15Zn**, **N3Zn**, **N4Zn**, **N5Zn**, **N8Zn**, **Si3-C**, **Si4-C**, **Si6-N**), 613 nm (**N6Zn**), 615 nm (**C6Zn**, **C7Zn**, **C14Zn**), 624 nm (**A9H**, **A10Al**, **N1Zn**, **N2Mg**, **N10Zn**, **N11Zn**, **Si5-N**), 625 nm (**A7Zn**, **A8Zn**), 630 nm (**C2Zn**, **C4Zn**, **C8Zn**, **C11Zn**, **N9Zn**), 635 nm (**A4Zn**), and 665 nm (**C9Zn**).

Determination of Quantum Yields of Singlet Oxygen Production

The quantum yields of singlet oxygen were calculated using the comparative method with unsubstituted zinc(II) phthalocyanine (ZnPc) as a reference ($\Phi_{\Delta(\mathrm{ZnPc})}$ = 0.56 in DMF[46]) and monitored using the decomposition of 1,3-diphenylisobenzofuran (DPBF) as a $^1O_2$ scavenger. The detailed procedure involved the transfer of 2.5 mL of stock solution of DPBF in DMF (5×10^{-5} M) into a 10 × 10 mm quartz cuvette, and it was bubbled with oxygen for 40 s. Eight μL of the 100 μM stock solution of the dye in DMF (or DMF + water or water; see above) was added. A xenon lamp (100 W, ozone free XE DC short arc lamp, New port) was used to irradiate the sample while stirring. The incident light was filtered through a water filter (6 cm) and cut off filter OG530 eliminating heat and light under 523 nm, respectively. For the porphyrin derivatives (**PpIX**, **verteporfin**, and **temoporfin**), a 20CGA-455 filter, and Rose Bengal (RB) as the reference ($\Phi_{\Delta(\mathrm{RB})}$ 0.68 in DMF[48]) were used. The decrease of DPBF in solution with irradiation time was monitored at 415 nm. The values of Φ_Δ of the dyes were calculated by the following equation:

$$\phi_\Delta^S = \phi_\Delta^R \left(\frac{k^S I_{aT}^R}{k^R I_{aT}^S} \right)$$

where k is the slope of the plot of the dependence of $\ln\left(\frac{A_0}{A_t}\right)$ on irradiation time t with A_0 and A_t being the absorbances of the DPBF at 415 nm before irradiation and after irradiation time t, respectively. I_{aT} is the total amount of light absorbed by the dye sample. Superscripts R and S indicate the reference and sample, respectively. I_{aT} is calculated as a sum of intensities of the absorbed light I_a at wavelengths from 523 to 850 nm (step 0.5 nm). Light under 523 nm is completely filtered by an OG530 filter, and light above 850 nm is not absorbed by the studied dye sample. I_a at a given wavelength is calculated using Beer–Lambert's law as

$$I_a = I_0(1 - e^{-2.3A})$$

https://doi.org/10.1021/acs.jmedchem.5c03090
J. Med. Chem. 2026, 69, 4391−4407

where I_0 is transmittance of the filter at the given wavelength and A is the absorbance of the dye at this wavelength. All experiments were performed three times, and the data presented is the mean value of the three obtained results with estimated error ± 10%.

Determination of Fluorescence Quantum Yields

The fluorescence quantum yields (Φ_F) were determined by a comparative method with ZnPc as the reference (Φ_F = 0.32 in THF[47]). The Φ_F values were calculated using the following formula:

$$\phi_F^S = \phi_F^R \left(\frac{F^S}{F^R}\right)\left(\frac{1-10^{-A^R}}{1-10^{-A^S}}\right)\left(\frac{\eta^S}{\eta^R}\right)^2$$

where F is the integrated area under the emission spectrum and A is the absorbance at the excitation wavelength. Superscripts R and S indicate the reference and sample, respectively. η stands for the refractive index of the solvent. Absorption in the Q-band was kept below 0.05 to eliminate the inner filter effect. Excitation wavelengths were the same as those used for emission spectra (see above). The emission wavelengths were set to their emission maxima to avoid exceeding the detector limit with stimated error ± 15%.

Study of Interaction with Bovine Serum Albumin (BSA)

To a 1 μM solution of the dye in PBS (0.01 M phosphate buffer, 0.0027 M potassium chloride, and 0.137 M sodium chloride, pH 7.4 in deionized water) in a quartz cuvette, prepared by dilution of the appropriate 100 μM stock solution of dye (see above), a 0.45 mM solution of BSA in PBS buffer was added sequentially to attain final concentrations of 17.5 μM, 35 μM, and 100 μM in the cuvette, and stirred for a few seconds at rt, and absorption and emission spectra were recorded after each addition.

Determination of Log *P*

400 μL portion of *n*-octanol and 400 μL of PBS buffer were mixed in a plastic Eppendorf vial. Then, 20 μL of the 100 μM stock solution of the sample (see above) was added to this mixture, vortexed for 5 min at rt, and then centrifuged for 10 min (10 000 rpm, rt). 50 μL of each of these layers was taken into 2.5 mL of DMF in a quartz cuvette, and their emission spectra (excitation wavelengths in Table 1) were recorded. The log *P* value was then computed using the area under the curve of the emission spectra of *n*-octanol (F_{oct}) and PBS buffer (F_{PBS}) layers as follows:

$$\log P = \log\left(\frac{F_{oct}}{F_{PBS}}\right)$$

Triplicate measurements were performed, and the data reported are the mean of the obtained results.

In Vitro Assessment of EC_{50} Values on HeLa, SK-MEL-28, and MCF-7 Cell Lines

For the cytotoxicity experiments (phototoxicity), cells were seeded at 100 μL per well into 96-well plates (TPP, Switzerland) at a density of 7.5×10^3 (HeLa) or 1.0×10^4 (MCF-7 and SK-MEL-28) cells per well. Cells were left to grow for 24 h (until they reached confluency) in a controlled environment of a CO_2 incubator (37 °C, 5% CO_2 atmosphere, constant high humidity). Subsequently, studied compounds were added in a wide concentration range and incubated with the cells for 12 h. Cells were washed; fresh cell culture medium was added, and the cells were irradiated using a 450 W Xe lamp (Newport, USA). The lamp was equipped with a long pass filter (Newport OG570) and an 8 cm water filter (λ > 570 nm, 12.4 mW/cm^2, 15 min, 11.2 J/cm^2). Cellular viability was assessed after an additional 24 h by the neutral red (NR; Sigma, Merck, USA) uptake assay. At least three independent experiments, each in triplicate, were performed. The soluble NR was measured at λ = 540 nm using a Tecan Infinite 200 M plate reader (Tecan, Austria). The viability of each experimental group was expressed as the percentage of the untreated cells (100% viability) after subtraction of the signal from cells treated with a lethal dose of hydrogen peroxide (0% viability). Results are shown on Figures S88–S93 and expressed as EC_{50} values (mean ± SD). EC_{50} values were calculated, and graphs were created by using GraphPad Prism 10.3.1 (Graph Pad software, USA).

Subcellular Localization on HeLa Cells

Approximately 7.5×10^4 HeLa cells were seeded on glass-bottom 35 mm Petri dishes suitable for confocal microscopy (WillCo Wells, The Netherlands) in SCM and incubated for 12 h with photosensitizers (concentration is listed in each respective image caption, Figures S94–S118) in a CO_2 incubator. The medium was removed, and the cells were washed twice with a prewarmed fresh medium. LysoTracker Blue DND-22 (0.3 μM; Molecular Probes, Thermofisher Scientific) and MitoTracker Green FM (0.3 μM; Molecular Probes, Thermofisher Scientific) were added, and the cells were incubated for an additional 15 min. After incubation, the cells were rinsed twice with prewarmed medium, and the samples were immediately examined using a Nikon Eclipse Ti-E (Nikon, Japan) fluorescence microscope equipped with an Andor Zyla 5.5 cooled digital sCMOS camera (Andor Technology, United Kingdom) and NIS Elements AR 5.3 software (Laboratory Imaging, Czech Republic). DAPI, FITC, and Cy5 filter sets were used for visualization. NIS Elements AR 5.3 software was also used to create fluorescence intensity profiles for each acquired data set. Analogical workflow was also used for the determination of subcellular localization to the cytoplasmic membrane. Instead of probes for mitochondria and lysosomes, probes for cytoplasmic membrane (1× CellMask Plasma Membrane Stain; Invitrogen, Thermofisher Scientific) and nuclei (10 nM Hoechst 33342; Invitrogen, Thermofisher Scientific) were used.

■ ASSOCIATED CONTENT

Data Availability Statement

The original photophysical data (absorption and emission spectra) and results from biological evaluation of the compounds have been deposited at Zenodo and are available at: https://zenodo.org/records/17284919.

Supporting Information

The Supporting Information is available free of charge at https://pubs.acs.org/doi/10.1021/acs.jmedchem.5c03090.

Absorption and emission spectra in DMF, water and PBS; changes in absorption and emission spectra upon interaction with BSA; *in vitro* assessment of EC_{50} values of HeLa, SK-MEL-28, and MCF-7 cell lines; subcellular localization on HeLa cells; graphs with statistical analysis; spectrum of lamp used for sample irradiation during *in vitro* studies (PDF)

Molecular formula strings and associated biological data (CSV)

■ AUTHOR INFORMATION

Corresponding Authors

Miloslav Machacek − *Faculty of Pharmacy in Hradec Kralove, Charles University, Hradec Kralove 500 03, Czech Republic;* orcid.org/0000-0001-7221-5914; Phone: +420 495067588; Email: machamil@faf.cuni.cz

Petr Zimcik − *Faculty of Pharmacy in Hradec Kralove, Charles University, Hradec Kralove 500 03, Czech Republic;* orcid.org/0000-0002-3533-3601; Phone: +420 495067257; Email: zimcik@faf.cuni.cz

Veronika Novakova − *Faculty of Pharmacy in Hradec Kralove, Charles University, Hradec Kralove 500 03, Czech Republic;* orcid.org/0000-0002-2183-1220; Phone: +420 495067257; Email: veronika.novakova@faf.cuni.cz

https://doi.org/10.1021/acs.jmedchem.5c03090
J. Med. Chem. 2026, 69, 4391−4407

Authors

Magdalena Kozlikova − *Faculty of Pharmacy in Hradec Kralove, Charles University, Hradec Kralove 500 03, Czech Republic*

Mary Angelia Alfred − *Faculty of Pharmacy in Hradec Kralove, Charles University, Hradec Kralove 500 03, Czech Republic*

Fabienne Dumoulin − *Faculty of Engineering and Natural Sciences, Department of Biomedical Engineering and Department of Chemistry, Acibadem Mehmet Ali Aydınlar University, Ataşehir, Istanbul 34752, Türkiye; Acibadem Mehmet Ali Aydinlar University, Graduate School of Natural and Applied Sciences, Ataşehir, Istanbul 34752, Türkiye;* orcid.org/0000-0002-0388-8338

Andrés de la Escosura − *Department of Organic Chemistry and Institute for Advanced Research in Chemistry (IAdChem), Universidad Autónoma de Madrid, 28049 Madrid, Spain;* orcid.org/0000-0002-0928-8317

Tomasz Goslinski − *Chair and Department of Chemical Technology of Drugs, Poznan University of Medical Sciences, 60-806 Poznań, Poland*

Marie Halaskova − *Faculty of Pharmacy in Hradec Kralove, Charles University, Hradec Kralove 500 03, Czech Republic*

Jian-Dong Huang − *College of Chemistry, Fujian Provincial Key Laboratory of Cancer Metastasis Chemoprevention and Chemotherapy, Fuzhou University, Fuzhou 350116, China;* orcid.org/0000-0003-0798-0147

Mei-Rong Ke − *College of Chemistry, Fujian Provincial Key Laboratory of Cancer Metastasis Chemoprevention and Chemotherapy, Fuzhou University, Fuzhou 350116, China;* orcid.org/0000-0002-0059-5919

Saad Makhseed − *Department of Chemistry, Kuwait University, Safat 13060, Kuwait;* orcid.org/0000-0002-3239-5524

Dariusz T. Mlynarczyk − *Chair and Department of Chemical Technology of Drugs, Poznan University of Medical Sciences, 60-806 Poznań, Poland;* orcid.org/0000-0003-3583-0752

Dennis K. P. Ng − *Department of Chemistry, The Chinese University of Hong Kong, Hong Kong 999077, China;* orcid.org/0000-0001-9087-960X

Tomás Torres − *Department of Organic Chemistry and Institute for Advanced Research in Chemistry (IAdChem), Universidad Autónoma de Madrid, 28049 Madrid, Spain; IMDEA-Nanociencia, 28049 Madrid, Spain;* orcid.org/0000-0001-9335-6935

Roy C. H. Wong − *Department of Chemistry, The Chinese University of Hong Kong, Hong Kong 999077, China*

Complete contact information is available at: https://pubs.acs.org/10.1021/acs.jmedchem.5c03090

Author Contributions

‡M.K., M.A.A., and M.M. contributed equally. The manuscript was written through contributions of all authors. All authors have given approval to the final version of the manuscript. P.Z. (conceptualization, writing−review and editing), F.D., A.E., T.G., J-D.H., M-R.K., S.M., D.K.P.N., R.C.H.W., D.T.M., and T.T. (resources), M.M. (methodology, investigation, supervision, formal analysis, writing−original draft), V.N. (methodology, investigation, supervision, writing−original draft, writing−review and editing), M.A.A., M.K., M.H. (investigation).

Notes

The authors declare no competing financial interest.

■ ACKNOWLEDGMENTS

The results were obtained with financial support from the Ministry of Education, Youth and Sports under the ERC CZ programme (project LL2318), the Czech Science Foundation (project 19-14758Y), and the project New Technologies for Translational Research in Pharmaceutical Sciences/NET-PHARM, project ID CZ.02.01.01/00/22_008/0004607, co-funded by the European Union. The financial support from Charles University (SVV 260 664 and 260 666) is gratefully acknowledged as well. A.E. and T.T. also acknowledge financial support from the Spanish MICIU/AEI/10.13039/501100011033/FEDER, UE (PID2023-151167NB-I00, PID2023-149983NB-I00), the Comunidad de Madrid and the Spanish State through the Recovery, Transformation and Resilience Plan ["Materiales Disruptivos Bidimensionales (2D)" (MAD2D-CM) (UAM1)-MRR Materiales Avanzados], and the European Union through the Next Generation EU funds. IMDEA Nanociencia is appreciative of support from the "Severo Ochoa" Programme for Centers of Excellence in R&D (CEX2020-001039-S). S.M. acknowledges the Kuwait Foundation for the Advancement of Science (KFAS) (grant no. P114-14-SC01). The authors would like to express their deep gratitude to the late Prof. Evgeny Lukyanets (2023) for providing *Pc* samples and for his significant contributions to the field. The meat grinder in the graphical abstract was generated using the Mind the Graph platform.

■ ABBREVIATIONS

$^1O_2$, singlet oxygen; BSA, bovine serum albumin; EC_{50}, half-maximal effective concentration; Pcs, phthalocyanines; PDT, photodynamic therapy; PS, photosensitizer; TLC, thin layer chromatography; Φ_Δ, quantum yield of singlet oxygen production; Φ_F, quantum yield of fluorescence; τ_F, fluorescence lifetime

■ REFERENCES

(1) Karges, J. Clinical Development of Metal Complexes as Photosensitizers for Photodynamic Therapy of Cancer. *Angew. Chem., Int. Ed.* **2022**, *61*, No. e202112236.

(2) Almeida-Marrero, V.; van de Winckel, E.; Anaya-Plaza, E.; Torres, T.; de la Escosura, A. Porphyrinoid biohybrid materials as an emerging toolbox for biomedical light management. *Chem. Soc. Rev.* **2018**, *47*, 7369−7400.

(3) Lo, P. C.; et al. The unique features and promises of phthalocyanines as advanced photosensitisers for photodynamic therapy of cancer. *Chem. Soc. Rev.* **2020**, *49*, 1041−1056.

(4) Rak, J.; Kabesova, M.; Benes, J.; Pouckova, P.; Vetvicka, D. Advances in Liposome-Encapsulated Phthalocyanines for Photodynamic Therapy. *Life* **2023**, *13*, 305.

(5) Li, D.; et al. Innovative Design Strategies Advance Biomedical Applications of Phthalocyanines. *Adv. Healthcare Mater.* **2023**, *12*, No. 2300263.

(6) de Siqueira, L. B. d. O.; et al. Pharmaceutical nanotechnology applied to phthalocyanines for the promotion of antimicrobial photodynamic therapy: A literature review. *Photodiagnosis and Photodynamic Therapy* **2022**, *39*, No. 102896.

(7) Liu, J.; et al. Nanoscale Covalent Organic Framework with Staggered Stacking of Phthalocyanines for Mitochondria-Targeted Photodynamic Therapy. *J. Am. Chem. Soc.* **2024**, *146*, 849−857.

(8) Peng, X. H.; et al. Comparison between amine-terminated phthalocyanines and their chlorambucil conjugates: Synthesis,

spectroscopic properties, and *in vitro* anticancer activity. *Tetrahedron* **2017**, *73*, 378−384.
(9) Pashkovskaya, A.; et al. Light-Triggered Liposomal Release: Membrane Permeabilization by Photodynamic Action. *Langmuir* **2010**, *26*, 5726−5733.
(10) Halaskova, M.; et al. Amphiphilic Cationic Phthalocyanines for Photodynamic Therapy of Cancer. *ChemPlusChem.* **2022**, *87*, No. e202200133.
(11) Svec, J.; et al. 1,2,5-Chalcogenadiazole-Annulated Tripyrazinoporphyrazines: Synthesis, Spectral Characteristics, and Influence of the Heavy Atom Effect on Their Photophysical Properties. *Eur. J. Org. Chem.* **2015**, *2015*, 596−604.
(12) Tuhl, A.; et al. Heavy metal effects on physicochemical properties of non-aggregated azaphthalocyanine derivatives. *J. Porphyrins Phthalocyanines* **2012**, *16*, 817−825.
(13) Azenha, E. G.; et al. Heavy-atom effects on metalloporphyrins and polyhalogenated porphyrins. *Chem. Phys.* **2002**, *280*, 177−190.
(14) Zou, J.; et al. BODIPY Derivatives for Photodynamic Therapy: Influence of Configuration versus Heavy Atom Effect. *Acs Appl. Mater. Inter* **2017**, *9*, 32475−32481.
(15) Repetowski, P.; et al. Synthesis, Photo-Characterizations, and Pre-Clinical Studies on Advanced Cellular and Animal Models of Zinc(II) and Platinum(II) Sulfonyl-Substituted Phthalocyanines for Enhanced Vascular-Targeted Photodynamic Therapy. *Acs Appl. Mater. Inter* **2024**, *16*, 48937−48954.
(16) Frochot, C.; Mordon, S. Update of the situation of clinical photodynamic therapy in Europe in the 2003−2018 period. *J. Porphyrins Phthalocyanines* **2019**, *23*, 347−357.
(17) Kollar, J.; et al. Cationic Versus Anionic Phthalocyanines for Photodynamic Therapy: What a Difference the Charge Makes. *J. Med. Chem.* **2020**, *63*, 7616−7632.
(18) Lan, W. L.; et al. The effects of formulation and serum albumin on the in vitro photodynamic activity of zinc(II) phthalocyanines substituted with sulfonated quinolineoxy groups. *Dyes Pigm.* **2016**, *128*, 215−225.
(19) Li, X. S.; et al. A non-aggregated and tumour-associated macrophage-targeted photosensitiser for photodynamic therapy: a novel zinc(II) phthalocyanine containing octa-sulphonates. *Chem. Commun.* **2015**, *51*, 4704−4707.
(20) Brilkina, A. A.; et al. Photobiological properties of phthalocyanine photosensitizers Photosens, Holosens and Phthalosens: A comparative in vitro analysis. *Journal of Photochemistry and Photobiology B-Biology* **2019**, *191*, 128−134.
(21) Ziental, D.; et al. Quaternized phthalocyanines as a tool against melanoma and a broad spectrum of bacteria and fungi. *Journal of Photochemistry and Photobiology B: Biology* **2025**, *268*, No. 113187.
(22) Anaya-Plaza, E.; et al. Synergy of Electrostatic and $\pi-\pi$ Interactions in the Realization of Nanoscale Artificial Photosynthetic Model Systems. *Angew. Chem., Int. Ed.* **2020**, *59*, 18786−18794.
(23) Anaya-Plaza, E.; et al. Photoantimicrobial Biohybrids by Supramolecular Immobilization of Cationic Phthalocyanines onto Cellulose Nanocrystals. *Chem.—Eur. J.* **2017**, *23*, 4320−4326.
(24) Halaskova, M.; et al. Peripherally Crowded Cationic Phthalocyanines as Efficient Photosensitizers for Photodynamic Therapy. *ACS Med. Chem. Lett.* **2021**, *12*, 502−507.
(25) Machacek, M.; et al. Far-Red-Absorbing Cationic Phthalocyanine Photosensitizers: Synthesis and Evaluation of the Photodynamic Anticancer Activity and the Mode of Cell Death Induction. *J. Med. Chem.* **2015**, *58*, 1736−1749.
(26) Makhseed, S.; et al. Water-soluble non-aggregating zinc phthalocyanine and in vitro studies for photodynamic therapy. *Chem. Commun.* **2013**, *49*, 11149−11151.
(27) Ghazal, B.; et al. Phthalocyanines and Tetrapyrazinoporphyrazines with Two Cationic Donuts: High Photodynamic Activity as a Result of Rigid Spatial Arrangement of Peripheral Substituents. *J. Med. Chem.* **2017**, *60*, 6060−6076.
(28) Liu, J.-Y.; Jiang, X.-J.; Fong, W.-P.; Ng, D. K. P. Highly photocytotoxic 1,4-dipegylated zinc(ii) phthalocyanines. Effects of the chain length on the in vitro photodynamic activities. *Organic & Biomolecular Chemistry* **2008**, *6*, 4560−4566.
(29) Mlynarczyk, D. T.; et al. Dendrimeric Sulfanyl Porphyrazines: Synthesis, Physico-Chemical Characterization, and Biological Activity for Potential Applications in Photodynamic Therapy. *ChemPlusChem.* **2016**, *81*, 460−470.
(30) Al-Hamdan, N. S.; et al. Enhanced photodynamic activity of asymmetric non-ionic Zn(II) phthalocyanine amphiphiles: Effect of molecular design on In vitro activity. *Dyes Pigm.* **2024**, *221*, No. 111809.
(31) Husain, A.; et al. Synthesis, Characterization, and Physicochemical Studies Of Orientation-Controlled Multi-Arm PEG Zn(II)/Mg(II) (Aza)Phthalocyanines. *ChemPlusChem.* **2022**, *87*, No. e202200275.
(32) Husain, A.; et al. Dually directional glycosylated phthalocyanines as extracellular red-emitting fluorescent probes. *Dalton Transactions* **2020**, *49*, 9605−9617.
(33) Zorlu, Y.; Dumoulin, F.; Durmus, M.; Ahsen, V. Comparative studies of photophysical and photochemical properties of solketal substituted platinum(II) and zinc(II) phthalocyanine sets. *Tetrahedron* **2010**, *66*, 3248−3258.
(34) Tuncel, S.; et al. Assessing the Dual Activity of a Chalcone−Phthalocyanine Conjugate: Design, Synthesis, and Antivascular and Photodynamic Properties. *Mol. Pharmaceutics* **2013**, *10*, 3706−3716.
(35) Jiang, X. J.; Yeung, S. L.; Lo, P. C.; Fong, W. P.; Ng, D. K. P. Phthalocyanine -Polyamine Conjugates as Highly Efficient Photosensitizers for Photodynamic Therapy. *J. Med. Chem.* **2011**, *54*, 320−330.
(36) Sun, Q.; et al. Highly photocytotoxic silicon(IV) phthalocyanines axially modified with l-tyrosine derivatives: Effects of mode of axial substituent connection and of formulation on photodynamic activity. *Dyes Pigm.* **2017**, *141*, 521−529.
(37) Novakova, V.; et al. Systematic investigation of phthalocyanines, naphthalocyanines, and their aza-analogues. Effect of the isosteric aza-replacement in the core. *Dalton Transactions* **2015**, *44*, 13220−13233.
(38) Kobayashi, N.; Ogata, H.; Nonaka, N.; Luk'yanets, E. A. Effect of peripheral substitution on the electronic absorption and fluorescence spectra of metal-free and zinc phthalocyanines. *Chem.—Eur. J.* **2003**, *9*, 5123−5134.
(39) Bunin, D. A.; Martynov, A. G.; Gvozdev, D. A.; Gorbunova, Y. G. Phthalocyanine aggregates in the photodynamic therapy: dogmas, controversies, and future prospects. *Biophysical Reviews* **2023**, *15*, 983−998.
(40) Liu, H.; et al. Phthalocyanine aggregates as semiconductor-like photocatalysts for hypoxic-tumor photodynamic immunotherapy. *Nat. Commun.* **2025**, *16*, 326.
(41) Li, M.; et al. New guidelines and definitions for type I photodynamic therapy. *Chem. Soc. Rev.* **2025**, *54*, 7025−7057.
(42) Zhao, P.-H.; et al. Aggregation-Enhanced Sonodynamic Activity of Phthalocyanine−Artesunate Conjugates. *Angew. Chem., Int. Ed.* **2022**, *61*, No. e202113506.
(43) Zhao, Y.-Y.; et al. Nanostructured Phthalocyanine Assemblies with Efficient Synergistic Effect of Type I Photoreaction and Photothermal Action to Overcome Tumor Hypoxia in Photodynamic Therapy. *J. Am. Chem. Soc.* **2021**, *143*, 13980−13989.
(44) Li, X.; et al. Supramolecular Phthalocyanine Assemblies for Improved Photoacoustic Imaging and Photothermal Therapy. *Angew. Chem., Int. Ed.* **2020**, *59*, 8630−8634.
(45) Lee, E.; et al. A boronic acid-functionalized phthalocyanine with an aggregation-enhanced photodynamic effect for combating antibiotic-resistant bacteria. *Chem. Sci.* **2020**, *11*, 5735−5739.
(46) Michelsen, U.; Kliesch, H.; Schnurpfeil, G.; Sobbi, A. K.; Wohrle, D. Unsymmetrically substituted benzonaphthoporphyrazines: A new class of cationic photosensitizers for the photodynamic therapy of cancer. *Photochem. Photobiol.* **1996**, *64*, 694−701.
(47) Zimcik, P.; et al. Magnesium Azaphthalocyanines: An Emerging Family of Excellent Red-Emitting Fluorophores. *Inorg. Chem.* **2012**, *51*, 4215−4223.

https://doi.org/10.1021/acs.jmedchem.5c03090
J. Med. Chem. 2026, 69, 4391−4407

(48) Redmond, R. W.; Gamlin, J. N. A compilation of singlet oxygen yields from biologically relevant molecules. *Photochem. Photobiol.* **1999**, *70*, 391−475.
(49) Novakova, V.; Donzello, M. P.; Ercolani, C.; Zimcik, P.; Stuzhin, P. A. Tetrapyrazinoporphyrazines and their metal derivatives. Part II: Electronic structure, electrochemical, spectral, photophysical and other application related properties. *Coord. Chem. Rev.* **2018**, *361*, 1−73.
(50) Novakova, V. Consequences of isosteric replacement of benzene for pyrazine in phthalocyanines. *J. Porphyrins Phthalocyanines* **2022**, *26*, 765−782.
(51) Zsila, F.; et al. Evaluation of drug−human serum albumin binding interactions with support vector machine aided online automated docking. *Bioinformatics* **2011**, *27*, 1806−1813.
(52) Li, X.; et al. In Vivo Albumin Traps Photosensitizer Monomers from Self-Assembled Phthalocyanine Nanovesicles: A Facile and Switchable Theranostic Approach. *J. Am. Chem. Soc.* **2019**, *141*, 1366−1372.
(53) Bunin, D. A.; et al. Pivotal Role of the Intracellular Microenvironment in the High Photodynamic Activity of Cationic Phthalocyanines. *J. Med. Chem.* **2025**, *68*, 658−673.
(54) Machacek, M.; et al. Anionic hexadeca-carboxylate tetrapyrazinoporphyrazine: synthesis and in vitro photodynamic studies of a water-soluble, non-aggregating photosensitizer. *RSC Adv.* **2016**, *6*, 10064−10077.
(55) Machacek, M.; et al. Tetra(3,4-pyrido)porphyrazines Caught in the Cationic Cage: Toward Nanomolar Active Photosensitizers. *J. Med. Chem.* **2016**, *59*, 9443−9456.
(56) Castano, A. P.; Demidova, T. N.; Hamblin, M. R. Mechanisms in photodynamic therapy: Part one - Photosensitizers, photochemistry and cellular localization. *Photodiagnosis and Photodynamic Therapy* **2004**, *1*, 279−293.
(57) Agostinis, P.; et al. Photodynamic therapy of cancer: An update. *CA: A Cancer Journal for Clinicians* **2011**, *61*, 250−281.
(58) Donohoe, C.; Senge, M. O.; Arnaut, L. G.; Gomes-da-Silva, L. C. Cell death in photodynamic therapy: From oxidative stress to anti-tumor immunity. *Bba-Rev. Cancer* **2019**, *1872*, 188308.
(59) Landry, J. J. M.; et al. The Genomic and Transcriptomic Landscape of a HeLa Cell Line. *G3 Genes|Genomes|Genetics* **2013**, *3*, 1213−1224.
(60) Krzemien, W.; et al. Tuning Photodynamic Properties of BODIPY Dyes, Porphyrins' Little Sisters. *Molecules* **2021**, *26*, 4194.
(61) Zhang, J.-X.; et al. A potential water-soluble ytterbium-based porphyrin−cyclen dual bio-probe for Golgi apparatus imaging and photodynamic therapy. *Chem. Commun.* **2012**, *48*, 9646−9648.
(62) Lai, S.-M.; et al. Enhanced Nuclear Localization of Photosensitizer Using Artificial Oil Bodies for Photodynamic Therapy. *Smart Science* **2016**, *4*, 167−172.
(63) Xiong, J.; Xue, E. Y.; Ng, D. K. P. Synthesis, Cellular Uptake, and Photodynamic Activity of Oligogalactosyl Zinc(II) Phthalocyanines. *ChemPlusChem.* **2023**, *88*, No. e202200285.
(64) Ge, W.; et al. Galactose-modified zinc phthalocyanines for colon cancer photodynamic therapy. *Photodiagnosis and Photodynamic Therapy* **2025**, *55*, No. 104765.

https://doi.org/10.1021/acs.jmedchem.5c03090
J. Med. Chem. 2026, 69, 4391−4407